follows: RNA was extracted from the Huh-7 culture supernatant using a QIAamp Viral RNA Kit (Qiagen, Valencia, CA, USA). The HCV RNA was quantified by real-time RT-PCR, using TaqMan EZ RT-PCR Core Reagents (Applied Biosystems) according to the manufacturer's protocol, using the published primers and probe [44]. The filtered (0.45 μm) culture supernatant of HCV-infected Huh-7 cells containing 2×10^8 HCV RNA copies/ml [equivalent to 9.7×10^4 focus-forming units (ffu)/ml] was used for the experiments. To analyze HCV-RNA in the supernatant, Huh-7 cells (2×10^5 cells in a 6-well plate) were infected with JFH-1 (multiplicity of infection [MOI] = 0.01) and after 4 h the cells were washed twice with phosphate-buffered saline (PBS). The supernatants were then collected and the cells were reseeded at 2×10^5 cells per 6-well plate. Then the HBV expression and mock plasmid were transfected by FuGENE6 (Roche Applied Science, IN, USA). The supernatant of the culture medium was collected 72 h after transfection. Quantification of HBV-DNA and HCV-RNA was carried out using real-time PCR.

IFN-α was added 24 h after the transfection of the HBV plasmids, and the supernatant of the culture medium was then collected 48 h after the addition of the IFN-α.

Results

Clinical characteristics of patients A and B

Patient A (high HBV-DNA titer and high HCV-RNA titer)

Patient A was a 44 year-old man with a high aspartate aminotransferase/alanine aminotransferase (AST/ALT) level. The prothrombin time-international normalized ratio (PT-INR) was in the normal range. Patient A had high HBV-DNA titers and high HCV-RNA titers (Table 1). His liver histology was classified as A2/F3 (Fig. 1). The laparoscopic analysis indicated moderate inflammation and intermediate fibrosis. The liver surfaces of the right lobe and left lobe were almost the same phenotype. Polymorphism of IL-28B (rs8099917) was T/G (hetero allele).

Patient B (low HBV-DNA titer and high HCV-RNA titer)

Patient B was a 63 year-old man with a low AST/ALT level. PT-INR was in the normal range. Patient B had low HBV-DNA titers and high HCV-RNA titers. The liver histology was classified as A2/F1 (Fig. 1). The liver surface showed moderate inflammation and was smooth. The polymorphism of IL-28B (rs8099917) was T/T (major homo allele).

Biopsy samples from patients with dual HBV and HCV infection were collected at the main liver centers in Miyagi prefecture. Fifteen HBV/HCV dual-infected patients were found in this study (Supplementary Table 1). Many of these patients had HCV-dominant infection and undetectable levels of HBV replication (10/15 patients). Most of the patients were HB envelope antigen (eAg)-negative and HBe antibody (Ab)-positive (14/14 patients). All HBV/HCV dual-infected patients who had received Peg-IFN-based

Table 1 Background of HBV/HCV dual-infected patients

	Patient A HCV high titer/ HBV high titer	Patient B HCV high titer/ HBV low titer	Normal range
Gender	Male	Male	
Age (years)	44	63	
HCV-RNA	6.5	5.5	log copies/ml
HCV genotype	1b	1b	
HBV-DNA	5.5	3.5	log copies/ml
HBV genotype	C	Bj	
HBe-Ag	129.5	0.5	0–0.9 index
HBe-Ab	0.1	99.3	0–49 %
Total bilirubin	0.7	1.2	0.2–1.2 mg/dl
Direct bilirubin	0.1	0.1	0–0.3 mg/dl
γ-GTP	208	31	8–57 IU/l
AST	138	33	12–30 IU/l
ALT	256	38	8–35 IU/l
Hb-A1c	5.3	5.4	4.3–5.8 %
Glu	103	83	68–106 mg/dl
BMI	25.34	18.75	
T-cho	160	195	128–220 mg/dl
LDL-cho	69	93	70–139 mg/dl
HDL-cho	37	67	36–89 md/dl
WBC	7800	5100	3200–9600/μl
RBC	491	446	428–566 × 10^4/μl
Hb	17.1	14.1	13.6–17.4 g/dl
PLT	169000	176000	155000–347000/μl
PT-INR	0.87	0.96	0–1.15 INR
Liver histology	A2/F3	A2/F1	METAVIR score
IL-28B SNP (rs8099917)	T/G	T/T	

HCV hepatitis C virus, *HBV* hepatitis B virus, e-*Ag* envelope antigen, *e-Ab* envelope antibody, *γ-GTP* γ-guanosine triphosphate, *AST* aspartate aminotransferase, *ALT* alanine aminotransferase, *Hb* hemoglobin, *Glu* glucose, *BMI* body mass index, *T-cho* total cholesterol, *LDL* low-density lipoprotein, *HDL* high-density lipoprotein, *PLT* platelets, *PT-INR* prothromin time-international normalized ratio, *IL* interleukin, *SNP* single-nucleotide polymorphism

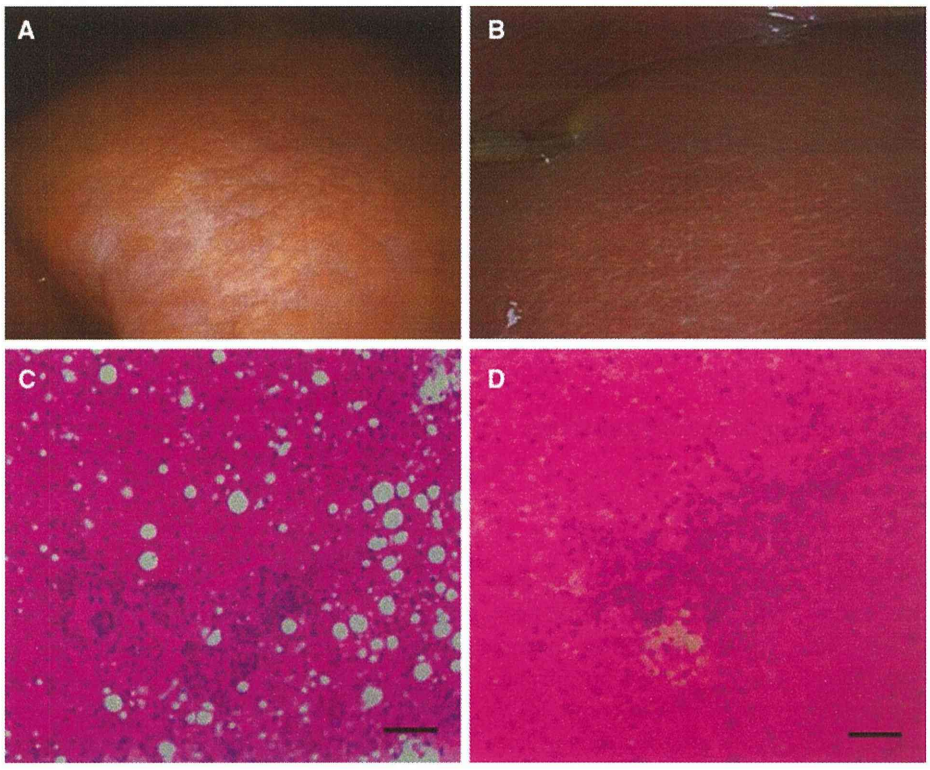

Fig. 1 Laparoscopic liver biopsy. The laparoscopic images of the liver surfaces of patient A (**a**) and patient B (**b**) are shown. Histopathology of patient A (**c**) and patient B (**d**) is also shown. *Bars* = 50 μm

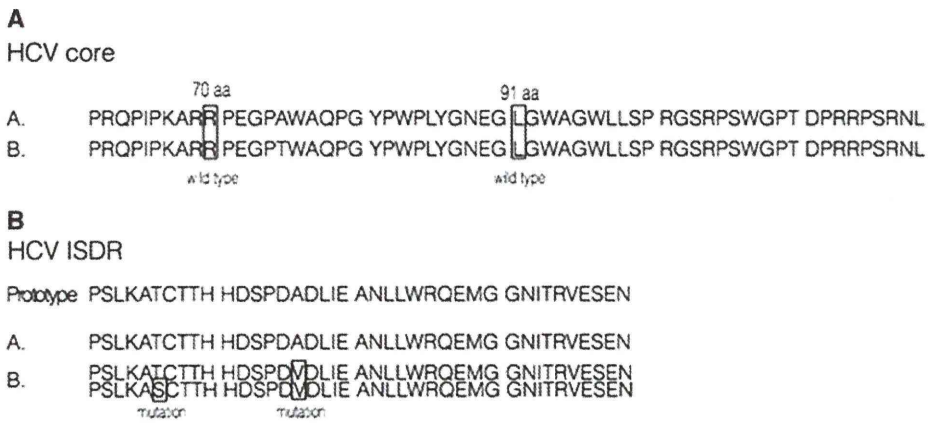

Fig. 2 Virological analysis of hepatitis B virus (HBV) and hepatitis C virus (HCV) in HBV/HCV dual infection. The amino acid sequences of the HCV-core region including core-70 and core-91, which were previously reported as determinants of the sensitivity to pegylated interferon/ribavirin (Peg-IFN/RBV) therapy, in patient A and patient B are shown (**a**). The amino acid sequences of the interferon sensitivity determining region (*ISDR*), which were previously reported as determinants of the sensitivity to IFN, in patients A and B are shown (**b**)

treatment achieved a sustained viral response (SVR) (5/5 patients). These data indicated that HCV-dominant dual-infected patients had good responses to treatment for HCV infection.

Virological analysis of HBV/HCV in patients A and B

The HCV genotype in both patient A and patient B was 1b. The sequences of amino acids in the ISDR region and HCV

core-70 and core-91 amino acids were analyzed by direct sequencing. Both patients had wild-type core-70 and core-91 amino acids (Fig. 2a). None of the mutations of the ISDR region was detected in patient A, but two of the mutations of the ISDR region were detected in patient B (Fig. 2b). The genotypes of HBV in patients A and B were analyzed by direct sequencing and phylogenetic tree analysis. The genotype of HBV in patient A was genotype C, which has been reported as difficult-to-treat HBV. The genotype of HBV in patient B was genotype Bj, which has been reported as easy-to-treat HBV in comparison to genotype C [45–47].

Sequential analysis of biochemical and virological data during Peg-IFN/RBV therapy

Patient A

In patient A, HCV-RNA gradually declined during Peg-IFN/RBV therapy. On the other hand, the HBV-DNA gradually increased during Peg-IFN/RBV therapy (Fig. 3a). The amount of HBeAg started to increase 9 months after the start of Peg-IFN/RBV therapy. HCV-RNA started to increase 12 months after the start of Peg-IFN/RBV therapy, although Peg-IFN/RBV was still being administered up to 18 months after the start of Peg-IFN/RBV therapy (Fig. 3a).

Patient B

In patient B, HCV-RNA and HBV-DNA rapidly declined after the start of Peg-IFN/RBV therapy (Fig. 3b). HCV-RNA could not be detected in peripheral blood 2 months after the start of Peg-IFN/RBV therapy. Peg-IFN/RBV was administered up to 12 months after the start of the Peg-IFN/RBV therapy. The amounts of HBeAb and HBeAg did not change during the Peg-IFN/RBV therapy (Fig. 3b).

Sequential immunological analysis during Peg-IFN/RBV therapy

We analyzed various subsets of immune cells that could affect the immunopathogenesis of HBV/HCV dual infection. NK cells ($CD3^-CD16^-CD56^{high}$ and $CD3^-CD16^+CD56^{dim}$) and NK-T cells ($CD3^+CD56^+CD16^+$, $CD3^+CD56^+CD16^-$ and $CD3^+CD56^-CD16^+$) were analyzed (Supplementary Fig. 1A). The $CD3^-$ gated lymphocytes were separated into 4 groups (a, b, c, and d). For these subsets, (a) indicated the presence of $CD3^-CD16^-CD56^{high}$ NK cells that could produce various cytokines vigorously and had low cytotoxic activity. Subset (b) showed $CD3^-CD16^+CD56^{dim}$ NK cells that had weak cytokine production ability and high cytotoxic activity.

The $CD3^+$ gated lymphocytes were separated into 3 groups (a, b, and c). The activated $CD3^+$, $CD3^+CD4^+$, and $CD3^+CD8^+$ T cells were analyzed (Supplementary Fig. 1B). HLA-DR^+ activated $CD3^+$, $CD3^+CD4^+$, and $CD3^+CD8^+$ T cells could be clearly distinguished by FACS analysis. Additionally, representative dot plots of Tregs and B cells were created (shown in Supplementary Fig. 1C). The frequencies of $CD3^-CD16^+CD56^{dim}$ NK cells, $CD3^+CD16^-CD56^+$ NK-T cells, activated $CD3^+CD4^+$ T cells, and activated $CD3^+CD8^+$ T cells fluctuated similarly during Peg-IFN/RBV therapy in patient A (Supplementary Fig. 1D). Activated T cells were increased at one month of Peg-IFN/RBV therapy, and the above subsets of lymphocytes gradually decreased up to 3 months of Peg-IFN/RBV therapy. After that, these cells gradually increased again up to 9 months of Peg-IFN/RBV therapy. In patient A, after 9 months of Peg-IFN/RBV therapy, these cells had decreased again (Supplementary Fig. 1D). The frequency of Tregs and activated B cells (data not shown) did not change during Peg-IFN/RBV therapy in patient A (Supplementary Fig. 1D). On the other hand, in patient B, the frequencies of $CD3^-CD16^+CD56^{dim}$ NK cells, $CD3^+CD16^-CD56^+$ NK-T cells, activated $CD3^+CD4^+$ T cells, and activated $CD3^+CD8^+$ T cells were increased and sustained during Peg-IFN/RBV therapy (Supplementary Fig. 1E). Five HCV monoinfected patients were analyzed by the same protocol (Supplementary Fig 1F). The mean frequency of various kinds of immune subsets was analyzed (Supplementary Fig 1F). The tendency of immunological reactions during Peg-IFN/RBV therapy in these five patients was similar to that in patient B.

Analysis of HBV- and HCV-specific immune responses

The analysis of HBV- and HCV-specific-immune responses was carried out by ELISPOT assay. Representative spots of IFN-γ are shown in Fig. 4a. In patient A, HCV- and HBV-specific IFN-γ secretion activities were remarkably low in comparison to the IL-10 secretion activity. Moreover, in patient A, the induction of IFN-γ-secreting cells could not be detected after Peg-IFN/RBV therapy, especially in regard to HBV-core specific IFN-γ secretion in PBMCs (Fig. 4b). On the other hand, in patient B, the HBV-core specific IFN-γ-secreting cells were high in comparison to those in patient A (Fig. 4c). Moreover, the induction of IFN-γ-secreting cells could be detected during Peg-IFN/RBV therapy in patient B (Fig. 4c). The mean numbers of IFN-γ- and IL-10-secreting spots in HBV-dominant dual-infected patients, patients with monoinfection with HBV genotype Bj ($HBeAb^+$), Bj ($HBeAg^+$), C ($HBeAb^+$), C ($HBeAg^+$), or HCV genotype 1b are shown in Fig. 4d. In patient A, HB core antigen (HBcAg)-specific IFN-γ secretion was weaker than that in

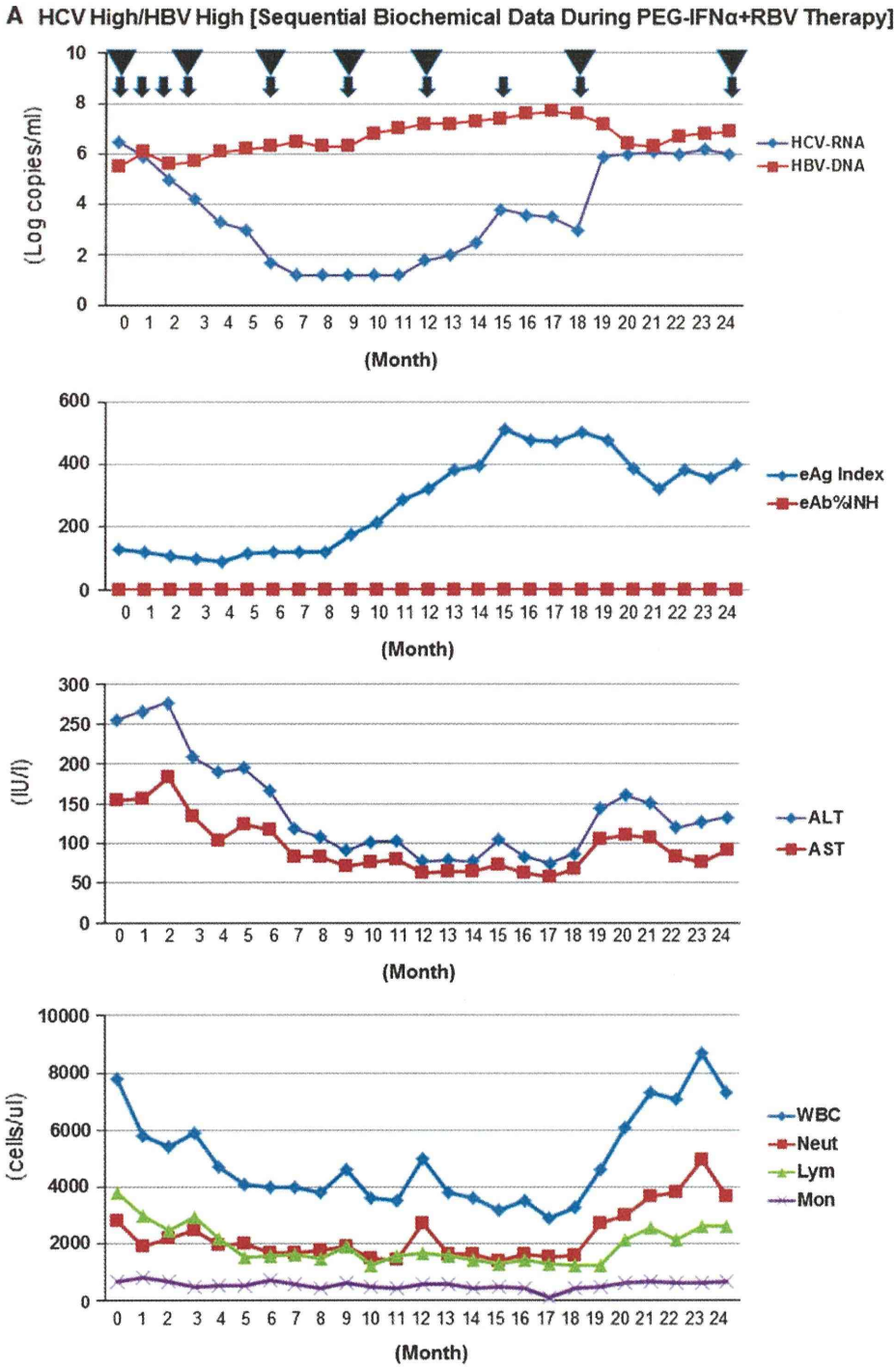

Fig. 3 Sequential biochemical data analysis during Peg-IFN/RBV therapy. The titers of HBV-DNA and HCV-RNA; the amounts of envelope antigen (*eAg*) and envelope antibody (*eAb*), and alanine aminotransferase (*ALT*) and aspartate aminotransferase (*AST*); and the numbers of WBCs, neutrophils (*Neut*), lymphocytes (*Lym*), and monocytes (*Mon*) in patients A (**a**) and B (**b**) are shown in these graphs. *Arrows* indicate the sampling points of FACS analysis. *Triangles* indicate the sampling points of the ELISPOT assay. *INH* inhibition

HBV-genotype C-monoinfected patients who were HBeAg-positive. However, HBcAg-specific IL-10 secretion in patient A was stronger than that in HBV-genotype C monoinfected patients who were HBeAg-positive. These data indicated that the presence of HCV might also suppress the HBV-specific immune response in regard to certain host factors (e.g., in the presence of IL-28B polymorphism, and depending on the body mass index [BMI] and γ-guanosine triphosphate [γ-GTP] level), because the presence of HCV did not suppress the HBV-specific immune response either in patient B or in the patients with dual HCV-dominant infection. Otherwise, we could deny the possibility indicating that

Fig. 3 continued

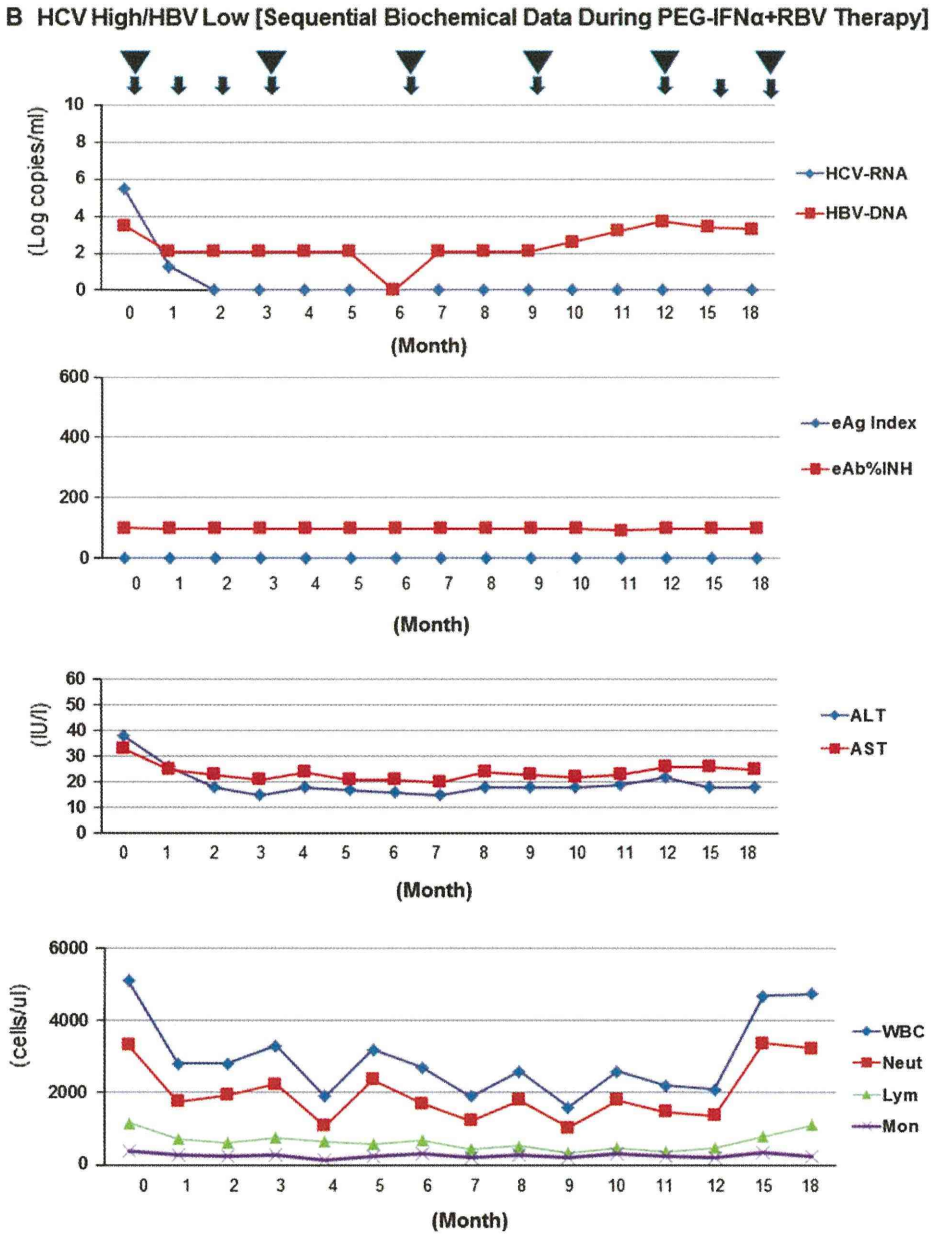

the certain background of host factors could allow the existence of dual virus actively. These data indicated that HBV-specific IL-10-secreting cells and/or certain kinds of host factors had an important role in HBV- and HCV-specific immune suppression in patient A, but not in patient B.

In vitro analysis of HBV/HCV dual infection

We carried out in vitro analysis of HBV/HCV infection using Huh-7 cells that were susceptible to the HCV-JFH-1 strain and HBV expression plasmids. The amount of the JFH-1 strain did not change with the various kinds of HBV expression plasmids (Fig. 5a). Moreover, the amounts of the various HBV strains did not change in the presence of JFH-1 infection. These data indicated that no direct effect of HBV and HCV could be detected in Huh 7 cells. We carried out experiments to analyze the effect of IFN-α treatment on HCV Huh-7 cells with various kinds of HBV expression (Fig. 5b). In our systems, it appeared that HBV expression could not significantly affect the suppressive effect of IFN-α.

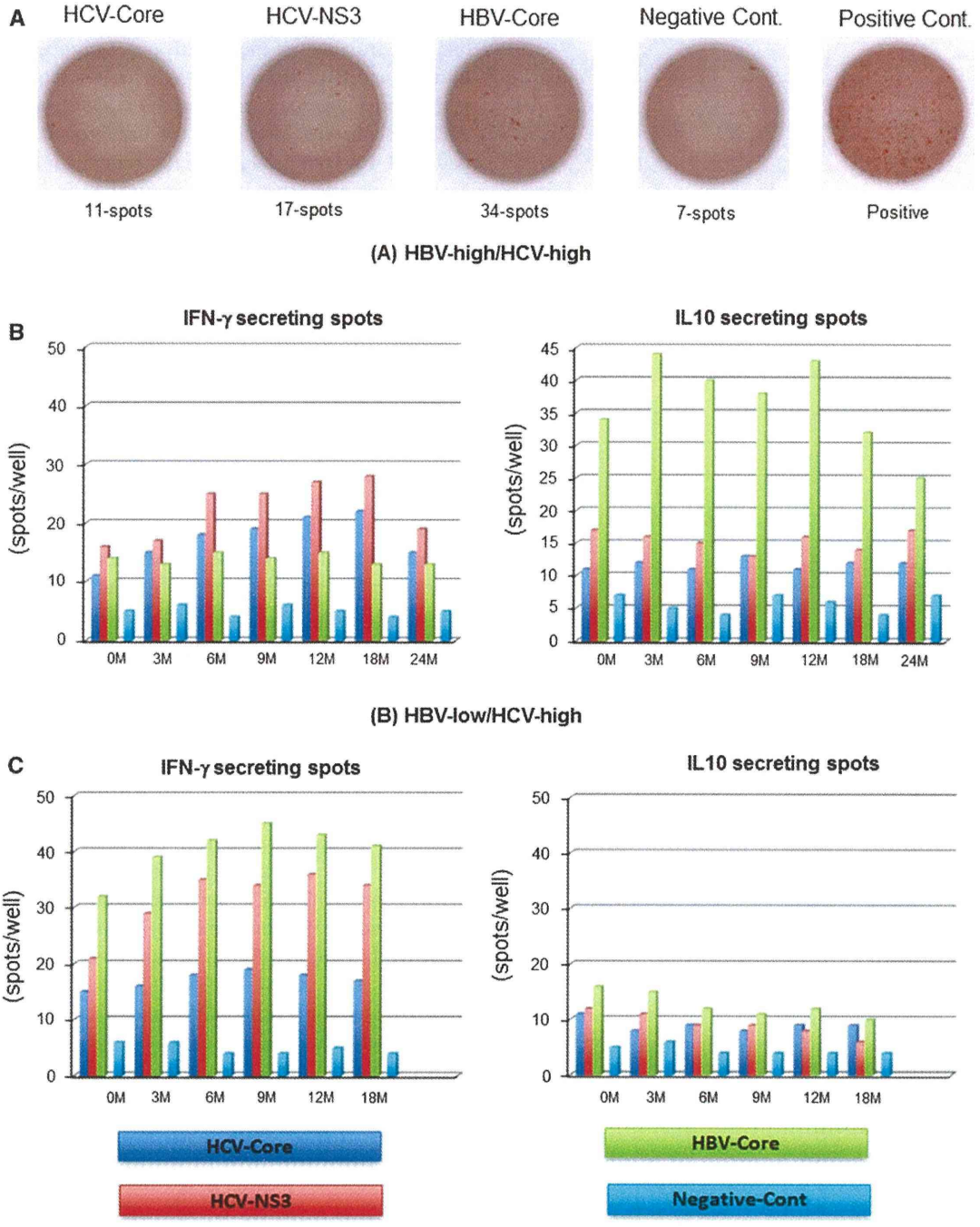

Fig. 4 The sequential analysis of HBV/HCV-specific immune reactions during Peg-IFN/RBV therapy. Representative spots of the ELISPOT assay are shown (**a**). The sequential data of IFN-γ- and interleukin-10 (*IL-10*)- secreting spots in patient A are shown (**b**). The sequential data of IFN-γ- and IL-10-secreting spots in patient B are shown (**c**). Comparison of IFN-γ- and IL-10- secreting spots in patient A before starting therapy, patient B before starting therapy, dual HCV-dominant patients, HCV-monoinfected patients, HBV-Bj ($HBeAb^+$) monoinfected patients, HBV-Bj ($HBeAg^+$) monoinfected patients, HBV-C ($HBeAb^+$) monoinfected patients, and HBV-C ($HBeAg^+$) monoinfected patients (**d**). In these *bar graphs*, the *blue bars* indicate HCV-core specific reaction. The *red bars* indicate HCV-NS3 specific reaction. The *green bars* indicate HBV-core specific reaction. The *aqua blue bars* indicate the negative control (*Cont.*). *Error bars* indicate standard deviations (color figure online)

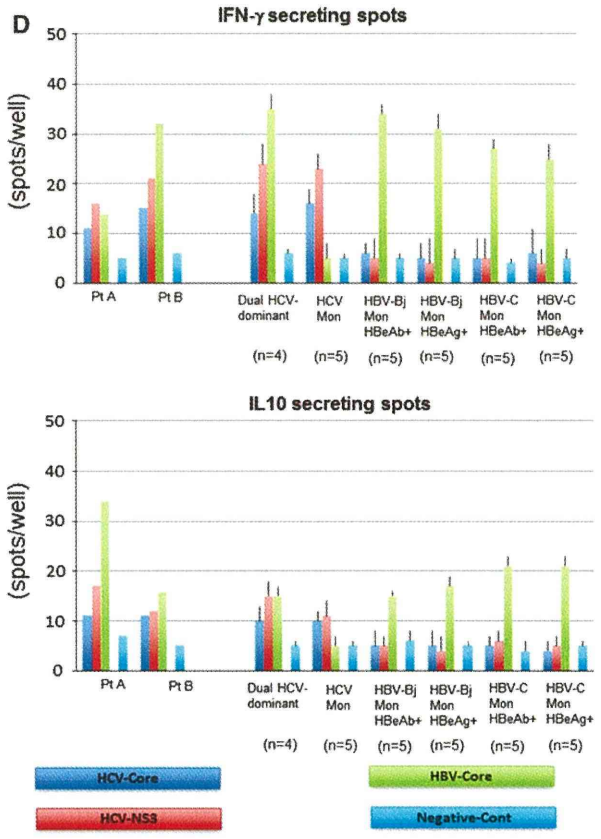

Fig. 4 continued

Discussion

The immunopathogenesis of dual hepatitis B and C infection is not clear, given the complexity of viral and host factors [19, 21, 48–50]. However, detailed understanding of specific patients with dual hepatitis B and C infection could contribute to improving the treatment and follow up of these patients. Therefore, we focused on two representative patients with HBV/HCV dual infection who received Peg-IFN/RBV therapy.

Concerning the virological results, patient A had genotype 1b, HCV-Core 70 wild-type and low mutation of ISDR HCV and genotype C HBV. It has been reported that genotype 1b HCV is common in Japan and is usually difficult to treat in comparison to genotypes 2a and 2b [51]. Among genotype 1b HCV strains, HCV-Core 70 wild-type HCV is easily decreased by Peg-IFN/RBV therapy [51]. On the other hand, it has been reported that in genotype 1b HCV low mutation of ISDR is difficult to treat [52]. Patient B had almost the same background of HCV–genotype 1b, HCV-Core 70 wild-type, and low mutation of ISDR–as patient A. However, the background of host factors that could affect the responsiveness of IFN-based therapy was different between patients A and B. For example, patient A had a hetero allele of the IL-28B polymorphism, advanced fibrosis, and fatty changes of the liver. On the other hand, patient B had the major allele of the IL-28B polymorphism and mild fibrosis. Moreover, the background of HBV in patient B was completely different from that in patient A. It has been reported that HBV genotype Bj is usually more susceptible to IFN-based therapy than genotype C [45, 53]. Therefore, not only the HBV factors but also the combination of host factors and HBV factors might affect the responsiveness to IFN-based therapy. In patient A, the responsiveness of HCV during Peg-IFN/RBV therapy was relatively poor. However, the viral titers of HCV were lower than 1.2 log copies/ml at 7 months after the start of therapy. During the reduction of the HCV viral titers, the titers of HBV and HBc-Ag specific IL-10-secreting cells were gradually increased. Although patient A had received Peg-IFN/RBV therapy for up to 18 months, HCV-RNA increased again 12 months after the start of the therapy. The sustained Th1 immune suppression might have contributed to the relapse of HCV. Not only weak up-regulation of HCV-specific Th1 immune reaction but also strong up-regulation of HBV-specific IL-10-secreting activity was detected during Peg-IFN/RBV therapy in patient A [26, 35]. Moreover, increased HBeAg could be detected 9 months after the start of the therapy. Fluctuations of activated CD4 cells, CD8 cells, NK cells, and NK-T cells could be seen in patient A. On the other hand, in patient B, the responsiveness of HBV and HCV during Peg-IFN/RBV therapy was good. Moreover, the immune response of patient B was almost comparable to the responses in the patients with HCV monoinfection and those with HBV-genotype Bj monoinfection. Previously, it has been reported that Peg-IFN/RBV therapy could achieve almost the same SVR rates in patients with HCV/HBV dual infection and those with HCV monoinfection [54–56]. We assume that the results in these studies were obtained from patients similar to our patient B, because the number of patients with HCV-dominant infection is much higher than the number of those with HBV/HCV dual active infection such as our patient A. Patients with HBV/HCV dual active infection such as patient A are relatively rare in Japan. However, it is necessary to understand the immunopathogenesis of these patients, because Peg-IFN/RBV therapy might not be sufficient to eradicate or control HBV/HCV in these difficult-to-treat patients. One of the candidate therapies for such patients might be Entecavir (ETV)/Peg-IFN/RBV sequential therapy. The effect of HBV specific regulatory T cells might contribute to the immunosuppression of not only HBV but also HCV [35]. In some previous studies, including ours, it has been reported that HBV replication might contribute to immune suppression [19, 29].

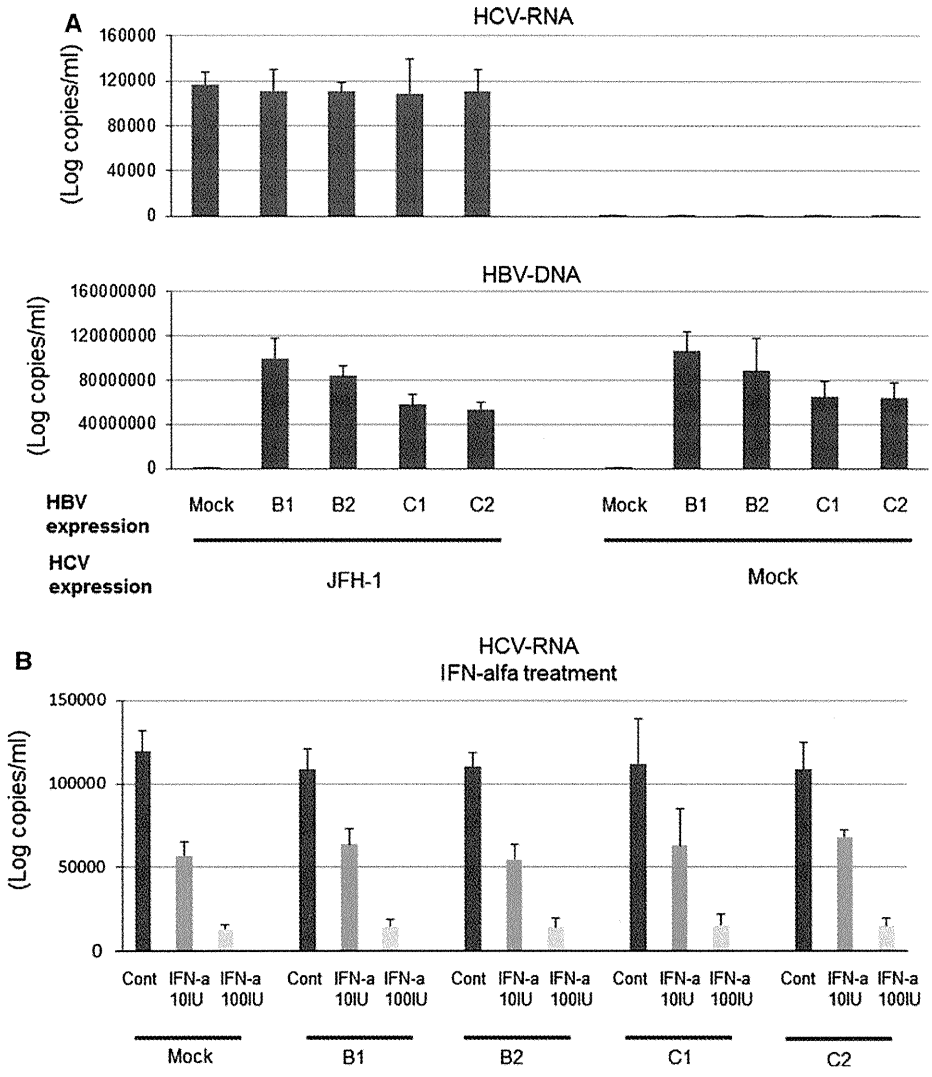

Fig. 5 In vitro analysis of HBV/HCV dual infection. The titers of HCV-RNA and HBV-DNA are shown. *B1* indicates genotype Bj35 clone. *B2* indicates genotype Bj56 clone. *C1* indicates genotype C-AT clone. *C2* indicates genotype C-22 clone (**a**). The titers of HCV-RNA after the IFN-α treatment are shown (**b**)

In the present study, we employed an in vitro coinfection system to analyze the direct interaction between HBV and HCV. In our system, we used several different HBV clones, because it is necessary to consider the effects of different genotypes. Although we could not detect the direct interaction of HBV/HCV in our system, we could not exclude the possibility of indirect interaction between cytokines and chemokines produced from virus-infected hepatocytes. We are now analyzing the chemokines produced from hepatoma cells with different HBV genotype clones (ongoing study).

In conclusion, we analyzed data from representative patients with HBV/HCV dual infection sequentially and precisely. Because many different kinds of backgrounds might affect immunoreactions, we focused on representative patients and analyzed the immunological responses extensively. There might be a group of patients with very difficult-to-treat dual infections. We need to understand the immunopathogenesis of such patients to develop the appropriate therapy.

Acknowledgments This work was supported in part by a Grant-in Aid from the Ministry of Education, Culture, Sport, Science, and Technology of Japan (Y.K. #23790761), and grants from the Ministry of Health, Labor, and Welfare of Japan.

Conflict of interest The authors declare that they have no conflict of interest.

References

1. Alter MJ, Kruszon-Moran D, Nainan OV, et al. The prevalence of hepatitis C virus infection in the United States, 1988 through 1994. N Engl J Med. 1999;341(8):556–62.

2. Tiollais P, Pourcel C, Dejean A. The hepatitis B virus. Nature. 1985;317(6037):489–95.
3. Lai CL, Ratziu V, Yuen MF, Poynard T. Viral hepatitis B. Lancet. 2003;362(9401):2089–94.
4. Poynard T, Yuen MF, Ratziu V, Lai CL. Viral hepatitis C. Lancet. 2003;362(9401):2095–100.
5. Potthoff A, Manns MP, Wedemeyer H. Treatment of HBV/HCV coinfection. Expert Opin Pharmacother. 2010;11(6):919–28.
6. Chu CJ, Lee SD. Hepatitis B virus/hepatitis C virus coinfection: epidemiology, clinical features, viral interactions and treatment. J Gastroenterol Hepatol. 2008;23(4):512–20.
7. Bini EJ, Perumalswami PV. Hepatitis B virus infection among American patients with chronic hepatitis C virus infection: prevalence, racial/ethnic differences, and viral interactions. Hepatology. 2010;51(3):759–66.
8. Halima SB, Bahri O, Maamouri N, et al. Serological and molecular expression of hepatitis B infection in patients with chronic hepatitis C from Tunisia, North Africa. Virol J. 2010;7:229.
9. Saravanan S, Velu V, Nandakumar S, et al. Hepatitis B virus and hepatitis C virus dual infection among patients with chronic liver disease. J Microbiol Immunol Infect. 2009;42(2):122–8.
10. Lee LP, Dai CY, Chuang WL, et al. Comparison of liver histopathology between chronic hepatitis C patients and chronic hepatitis B and C-coinfected patients. J Gastroenterol Hepatol. 2007;22(4):515–7.
11. Liu Z, Hou J. Hepatitis B virus (HBV) and hepatitis C virus (HCV) dual infection. Int J Med Sci. 2006;3(2):57–62.
12. Tsai JF, Jeng JE, Ho MS, et al. Effect of hepatitis C and B virus infection on risk of hepatocellular carcinoma: a prospective study. Br J Cancer. 1997;76(7):968–74.
13. Cho LY, Yang JJ, Ko KP, et al. Coinfection of hepatitis B and C viruses and risk of hepatocellular carcinoma: systematic review and meta-analysis. Int J Cancer. 2011;128(1):176–84.
14. Huo TI, Huang YH, Hsia CY, et al. Characteristics and outcome of patients with dual hepatitis B and C-associated hepatocellular carcinoma: are they different from patients with single virus infection? Liver Int. 2009;29(5):767–73.
15. Kew MC. Interaction between hepatitis B and C viruses in hepatocellular carcinogenesis. J Viral Hepat. 2006;13(3):145–9.
16. Liu CJ, Chen PJ, Chen DS. Dual chronic hepatitis B virus and hepatitis C virus infection. Hepatol Int. 2009;3(4):517–25.
17. Bellecave P, Gouttenoire J, Gajer M, et al. Hepatitis B and C virus coinfection: a novel model system reveals the absence of direct viral interference. Hepatology. 2009;50(1):46–55.
18. Eyre NS, Phillips RJ, Bowden S, et al. Hepatitis B virus and hepatitis C virus interaction in Huh-7 cells. J Hepatol. 2009;51(3):446–57.
19. Chisari FV, Ferrari C. Hepatitis B virus immunopathogenesis. Annu Rev Immunol. 1995;13:29–60.
20. Koziel MJ. The role of immune responses in the pathogenesis of hepatitis C virus infection. J Viral Hepat. 1997;4(Suppl 2):31–41.
21. Rice CM, Walker CM. Hepatitis C virus-specific T lymphocyte responses. Curr Opin Immunol. 1995;7(4):532–8.
22. Nan XP, Zhang Y, Yu HT, et al. Circulating $CD4^{+}CD25^{high}$ regulatory T cells and expression of PD-1 and BTLA on $CD4^{+}$ T cells in patients with chronic hepatitis B virus infection. Viral Immunol. 2010;23(1):63–70.
23. Kondo Y, Ueno Y, Shimosegawa T. Immunopathogenesis of hepatitis B persistent infection: implications for immunotherapeutic strategies. Clin J Gastroenterol. 2009;2(2):71–9.
24. Peng G, Li S, Wu W, Sun Z, Chen Y, Chen Z. Circulating $CD4^{+}$ $CD25^{+}$ regulatory T cells correlate with chronic hepatitis B infection. Immunology. 2008;123(1):57–65.
25. Maier H, Isogawa M, Freeman GJ, Chisari FV. PD-1:PD-L1 interactions contribute to the functional suppression of virus-specific $CD8^{+}$ T lymphocytes in the liver. J Immunol. 2007;178(5):2714–20.
26. Kondo Y, Kobayashi K, Ueno Y, et al. Mechanism of T cell hyporesponsiveness to HBcAg is associated with regulatory T cells in chronic hepatitis B. World J Gastroenterol. 2006;12(27):4310–7.
27. Stoop JN, van der Molen RG, Baan CC, et al. Regulatory T cells contribute to the impaired immune response in patients with chronic hepatitis B virus infection. Hepatology. 2005;41(4):771–8.
28. Kondo Y, Kobayashi K, Asabe S, et al. Vigorous response of cytotoxic T lymphocytes associated with systemic activation of CD8 T lymphocytes in fulminant hepatitis B. Liver Int. 2004;24(6):561–7.
29. Kondo Y, Asabe S, Kobayashi K, et al. Recovery of functional cytotoxic T lymphocytes during lamivudine therapy by acquiring multi-specificity. J Med Virol. 2004;74(3):425–33.
30. Kondo Y, Ueno Y, Kakazu E, et al. Lymphotropic HCV strain can infect human primary naive CD4(+) cells and affect their proliferation and IFN-gamma secretion activity. J Gastroenterol. 2011;46:232–41.
31. Kondo Y, Machida K, Liu HM, et al. Hepatitis C virus infection of T cells inhibits proliferation and enhances fas-mediated apoptosis by down-regulating the expression of CD44 splicing variant 6. J Infect Dis. 2009;199(5):726–36.
32. Kondo Y, Sung VM, Machida K, Liu M, Lai MM. Hepatitis C virus infects T cells and affects interferon-gamma signaling in T cell lines. Virology. 2007;361(1):161–73.
33. Ulsenheimer A, Gerlach JT, Gruener NH, et al. Detection of functionally altered hepatitis C virus-specific CD4 T cells in acute and chronic hepatitis C. Hepatology. 2003;37(5):1189–98.
34. Cramp ME, Rossol S, Chokshi S, Carucci P, Williams R, Naoumov NV. Hepatitis C virus-specific T-cell reactivity during interferon and ribavirin treatment in chronic hepatitis C. Gastroenterology. 2000;118(2):346–55.
35. Kondo Y, Ueno Y, Kobayashi K, et al. Hepatitis B virus replication could enhance regulatory T cell activity by producing soluble heat shock protein 60 from hepatocytes. J Infect Dis. 2010;202(2):202–13.
36. Nguyen LH, Ko S, Wong SS, et al. Ethnic differences in viral dominance patterns in patients with hepatitis B virus and hepatitis C virus dual infection. Hepatology. 2011;53(6):1839–45.
37. Takahashi M, Nishizawa T, Gotanda Y, et al. High prevalence of antibodies to hepatitis A and E viruses and viremia of hepatitis B, C, and D viruses among apparently healthy populations in Mongolia. Clin Diagn Lab Immunol. 2004;11(2):392–8.
38. Ina Y. ODEN: a program package for molecular evolutionary analysis and database search of DNA and amino acid sequences. Comput Appl Biosci. 1994;10(1):11–2.
39. Thompson JD, Higgins DG, Gibson TJ. CLUSTAL W: improving the sensitivity of progressive multiple sequence alignment through sequence weighting, position-specific gap penalties and weight matrix choice. Nucleic Acids Res. 1994;22(22):4673–80.
40. Saitou N, Nei M. The neighbor-joining method: a new method for reconstructing phylogenetic trees. Mol Biol Evol. 1987;4(4):406–25.
41. Felsenstein J. Estimating effective population size from samples of sequences: a bootstrap Monte Carlo integration method. Genet Res. 1992;60(3):209–20.
42. Perriere G, Gouy M. WWW-query: an on-line retrieval system for biological sequence banks. Biochimie. 1996;78(5):364–9.
43. Wakita T, Pietschmann T, Kato T, et al. Production of infectious hepatitis C virus in tissue culture from a cloned viral genome. Nat Med. 2005;11(7):791–6.
44. Takeuchi T, Katsume A, Tanaka T, et al. Real-time detection system for quantification of hepatitis C virus genome. Gastroenterology. 1999;116(3):636–42.

45. Sugauchi F, Kumada H, Sakugawa H, et al. Two subtypes of genotype B (Ba and Bj) of hepatitis B virus in Japan. Clin Infect Dis. 2004;38(9):1222–8.
46. Sugauchi F, Orito E, Ichida T, et al. Epidemiologic and virologic characteristics of hepatitis B virus genotype B having the recombination with genotype C. Gastroenterology. 2003; 124(4):925–32.
47. Orito E, Mizokami M, Sakugawa H, et al. A case–control study for clinical and molecular biological differences between hepatitis B viruses of genotypes B and C. Japan HBV Genotype Research Group. Hepatology. 2001;33(1):218–23.
48. Raimondo G, Brunetto MR, Pontisso P, et al. Longitudinal evaluation reveals a complex spectrum of virological profiles in hepatitis B virus/hepatitis C virus-coinfected patients. Hepatology. 2006;43(1):100–7.
49. Chuang WL, Dai CY, Chang WY, et al. Viral interaction and responses in chronic hepatitis C and B coinfected patients with interferon-alpha plus ribavirin combination therapy. Antivir Ther. 2005;10(1):125–33.
50. Tsai SL, Liaw YF, Yeh CT, Chu CM, Kuo GC. Cellular immune responses in patients with dual infection of hepatitis B and C viruses: dominant role of hepatitis C virus. Hepatology. 1995;21(4):908–12.
51. Akuta N, Suzuki F, Hirakawa M, et al. Amino acid substitution in hepatitis C virus core region and genetic variation near the interleukin 28B gene predict viral response to telaprevir with peginterferon and ribavirin. Hepatology. 2010;52(2):421–9.
52. Fukuma T, Enomoto N, Marumo F, Sato C. Mutations in the interferon-sensitivity determining region of hepatitis C virus and transcriptional activity of the nonstructural region 5A protein. Hepatology. 1998;28(4):1147–53.
53. Akuta N, Kumada H. Influence of hepatitis B virus genotypes on the response to antiviral therapies. J Antimicrob Chemother. 2005;55(2):139–42.
54. Yu ML, Lee CM, Chuang WL, et al. HBsAg profiles in patients receiving peginterferon alfa-2a plus ribavirin for the treatment of dual chronic infection with hepatitis B and C viruses. J Infect Dis. 2010;202(1):86–92.
55. Yu JW, Sun LJ, Zhao YH, Kang P, Gao J, Li SC. Analysis of the efficacy of treatment with peginterferon alpha-2a and ribavirin in patients coinfected with hepatitis B virus and hepatitis C virus. Liver Int. 2009;29(10):1485–93.
56. Liu CJ, Chuang WL, Lee CM, et al. Peginterferon alfa-2a plus ribavirin for the treatment of dual chronic infection with hepatitis B and C viruses. Gastroenterology. 2009;136((2)):496.e3–504.e3.

Biochemical and Biophysical Research Communications xxx (2011) xxx–xxx

Contents lists available at ScienceDirect

Biochemical and Biophysical Research Communications

journal homepage: www.elsevier.com/locate/ybbrc

AMSH is required to degrade ubiquitinated proteins in the central nervous system

Shunya Suzuki [a], Keiichi Tamai [a,d,*], Masahiko Watanabe [e], Masanao Kyuuma [a], Masao Ono [c], Kazuo Sugamura [a,d], Nobuyuki Tanaka [b,d]

[a] Department of Microbiology and Immunology, Tohoku University Graduate School of Medicine, Sendai 980-8575, Japan
[b] Department of Cancer Science, Tohoku University Graduate School of Medicine, Sendai 980-8575, Japan
[c] Department of Pathology, Tohoku University Graduate School of Medicine, Sendai 980-8575, Japan
[d] Division of Immunology, Miyagi Cancer Center Research Institute, Natori 981-1293, Japan
[e] Department of Anatomy, Hokkaido University School of Medicine, Sapporo 060-8638, Japan

ARTICLE INFO

Article history:
Received 14 April 2011
Available online xxxx

Keywords:
AMSH
Neurodegeneration
Ubiquitin
Hippocampus

ABSTRACT

Deubiquitination is a biochemical process that mediates the removal of ubiquitin moieties from ubiquitin-conjugated substrates. AMSH (associated molecule with the SH3 domain of STAM) is a deubiquitination enzyme that participates in the endosomal sorting of several cell-surface molecules. AMSH impairment results in missorted ubiquitinated cargoes *in vitro* and severe neurodegeneration *in vivo*, but it is not known how AMSH deficiency causes neuronal damage in the brain. Here, we demonstrate that AMSH$^{-/-}$ mice developed ubiquitinated protein accumulations as early as embryonic day 10 (E10), and that severe deposits were present in the brain at postnatal day 8 (P8) and P18. Interestingly, TDP-43 was found to accumulate and colocalize with glial marker-positive cells in the brain. Glutamate receptor and p62 accumulations were also found; these molecules colocalized with ubiquitinated aggregates in the brain. These data suggest that AMSH plays an important role in degrading ubiquitinated proteins and glutamate receptors *in vivo*. AMSH$^{-/-}$ mice provide an animal model for neurodegenerative diseases, which are commonly characterized by the generation of proteinaceous aggregates.

© 2011 Elsevier Inc. All rights reserved.

1. Introduction

The highly dynamic endosomal sorting process determines a membrane-bound protein's fate by either recycling it back to the cell surface or delivering it into endosomal network pathways. Membrane proteins destined for lysosomes are tagged with ubiquitin. Endosomal sorting complexes required for transport (ESCRT) recognizes and dictates cargo selection. ESCRT produces intraluminal vesicles (ILVs) that originate by inward budding from the limiting membrane of the sorting endosome [1]. This process creates a multivesicular body (MVB), which leads to lysosome-dependent cargo degradation through the subsequent MVB-lysosome fusion event.

Balanced ubiquitination and deubiquitination of cargos is a prerequisite for protein homeostasis. Ubiquitin modifications are reversed through the isopeptidase activities of deubiquitinating enzymes (DUBs), with most of the DUBs studied deconjugating only a small number of targets [2]. In fact, deubiquitination, a term used here to refer to both ubiquitin and ubiquitin-like deconjugation, is emerging as a regulatory process in signaling pathways, chromatin structure, endocytosis, and apoptosis [2], and is important for physiological activities such as development, immunity, and neuronal function [3].

We identified AMSH (associated molecule with the SH3 domain of STAM) [4] while screening for an ESCRT-bound molecule. AMSH is an endosomal DUB in the JAMM metalloprotease family, and plays a role in MVB/late endosomes. Recombinant AMSH has been shown to deubiquitinate epidermal growth factor receptor (EGFR) and to cleave lysine 63 (K63)-linked, but not lysine 48 (K48)-linked, polyubiquitin chains into ubiquitin monomers [5]. In a previous study, we found that AMSH binds the ESCRT-III subunit CHMP3 and plays a role in MVB/late endosomes [6]. AMSH also binds the ESCRT-III subunits CHMP1A, CHMP1B, and CHMP2A [7]. This intimate relationship between AMSH and ESCRT prompted us to investigate AMSH's *in vivo* roles. We have reported that AMSH knockout mice (AMSH$^{-/-}$) exhibit postnatal growth retardation and die between postnatal day 19 (P19) and P23. AMSH$^{-/-}$ mice exhibit severe neuronal damage, specifically neuron loss and increasing numbers of apoptotic cells, that is almost en-

Abbreviations: AD, Alzheimer's disease; ALS, amyotrophic lateral sclerosis; AMSH, associated molecule with the SH3 domain of STAM; AMPAR, α-amino-3-hydroxy-5-methyl-isoxazolepropionic acid receptor; CHMP, chromatin modifying protein; ESCRT, endosomal sorting complexes required for transport; FTD, frontotemporal dementia; MVB, multivesicular body; NMDAR, *N*-methyl-D-aspartate receptor; PD, Parkinson's disease; DUB, deubiquitinating enzyme.

* Corresponding author at: Division of Immunology, Miyagi Cancer Center Research Institute, 47-1 Nodayama, Medeshima-Shiode, Natori, Miyagi 981-1293, Japan. Fax: +81 22 381 1168.
E-mail address: tamaikeiichi@mac.com (K. Tamai).

0006-291X/$ - see front matter © 2011 Elsevier Inc. All rights reserved.
doi:10.1016/j.bbrc.2011.04.065

tirely confined to the CA1 subfield of the hippocampus [8]. Despite the severity of these AMSH-deficient neuronal phenotypes, the pathophysiology is not fully understood.

Most age-related neurodegenerative diseases are characterized by accumulations of aberrant protein aggregates in affected regions of the brain. In particular, ubiquitin-positive proteinaceous deposits are a hallmark of neurodegeneration; such deposits include Lewy bodies in Parkinson's disease (PD), neurofibrillary tangles in Alzheimer disease (AD), Bunina bodies in amyotrophic lateral sclerosis (ALS), and Pick bodies in frontotemporal dementia (FTD) with parkinsonism [9]. Since principal function of ubiquitination is to maintain protein homeostasis inside a cell, these neuronal pathologies may indicate a failure to clear unwanted proteins [9]. A recent report suggests that ESCRT-III dysfunction is associated with neurodegeneration resembling age-dependent neurodegenerative diseases such as FTD [10]. A certain percentage of FTD is known as chromosome 3-linked FTD (FTD3), which is attributed to a genetic disorder or mutation of the ESCRT-III molecule CHMP2B [11]. In a previous study using neuron-specific knockout mice, we found that the ESCRT-0 protein Hrs plays a pivotal role in neural cell survival by clearing ubiquitinated proteins in neurons [12]. A growing body of evidence suggests that insufficient ESCRT function leads to the accumulation of ubiquitinated proteins and to human neurodegenerative disease [13]. Nevertheless, little is known about how an ESCRT-associating DUB is involved in ubiquitinated protein degradation in the central nervous system. Here, we demonstrate that ubiquitinated protein accumulations are present in brain lesions found in AMSH$^{-/-}$ mice, and that AMSH is crucial for the proper degradation of both ubiquitinated proteins and glutamate receptors in the central nervous system.

2. Materials and methods

2.1. Cell fractionation

Cerebral tissues were washed with phosphate-buffered saline (PBS), suspended with homogenization buffer (10 mM HEPES, 3 mM imidazole, and 250 mM sucrose), and dissociated by passage through a 22-G needle. The cells were centrifuged at 3000*g* for 10 min at 4 °C, and the supernatants were ultracentrifuged at 100,000*g* for 30 min at 4 °C. The supernatants were regarded as the cytoplasmic fraction, and the pellets as the membrane fraction. The pellets were resuspended with IP buffer (10 mM Hepes, pH 7.2, 0.5% Triton-X, 150 mM NaCl) and centrifuged at 10,000*g* for 30 min at 4 °C. The supernatants were filtered through a polyvinylidene difluoride (PVDF) membrane (0.45 μm, PALL Life Sciences, NY) and regarded as a membrane fraction. These fractions were quantified using the Bio-Rad Protein assay (Bio-Rad, CA) according to the manufacturer's protocol.

2.2. Western blotting

Immunoblotting was conducted as previously described [4]. In brief, mouse brain lysates were fractionated as described above, then separated by sodium dodecyl sulfate–polyacrylamide gel electrophoresis (SDS–PAGE) and transferred onto PVDF membranes (Millipore, MA). After being blocked with 5% nonfat milk in Tris-buffered saline (TBS) containing 0.1% Tween 20, the membranes were probed with the primary antibodies indicated below, washed again, and probed with horseradish peroxidase (HRP)-conjugated secondary antibodies (Cell Signaling, MA).

2.3. Immunofluorescence reactions and immunohistochemistry

For immunofluorescence studies, mice were perfused with 4% paraformaldehyde, and 50-μm sections were prepared using a microslicer (VT1000S, Leica, Nussloch, Germany). The antibodies and dilutions used were as follows: Anti-ubiquitin mouse monoclonal Ab (mAb) 1B3 (MBL, Nagoya, Japan), 1:100; anti-ubiquitin mouse mAb FK2 (BIOMOL, NY), 1:100; anti-TDP-43 mouse mAb (TARDBP) (Proteintech Group, IL), 1:100; anti-p62 (C-terminal specific) guinea pig polyclonal antibody (pAb) (American Research Products, MA), 1:100; anti-GFAP mouse mAb (Chemicon, CA), 1:200; anti-tyrosine hydroxylase rabbit pAb (AB152, Chemicon), 1:1000; anti-microtubule-associated protein 2 goat pAb (MAP2, [14]), 1 μg/mL; anti-calbindin rabbit pAb [15], 1 μg/mL. Appropriately, coupled secondary antibodies (Alexa Fluor, Molecular Probes, CA) were used for double-labeling. For immunohistochemistry, we used the Histofine mouse stain kit or Histofine simple stain mouse MAX-PO(R) (Nichirei, Japan), according to the manufacturer's protocols.

3. Results

Because AMSH is a deubiquitinating enzyme with endosome functions, we analyzed ubiquitinated protein accumulation in the soluble (cytoplasmic) and insoluble (membrane) fractions of the AMSH$^{-/-}$ brain. Western blot analysis using the anti-ubiquitin antibody P4D1 revealed no difference in ubiquitinated protein levels in the soluble fractions from control or AMSH$^{-/-}$ brains (Fig. 1, left panels). In the insoluble fraction, however, the ubiquitinated protein levels were higher in the AMSH$^{-/-}$ brain than in the control (Fig. 1, right panels). The ubiquitinated protein levels in the insoluble fraction increased slightly from embryonic day 10 (E10) to postnatal day 8 (P8) in the control brain, and the levels were higher in the AMSH$^{-/-}$ than the control brain during E10 to P18, near the end of the AMSH$^{-/-}$ mouse lifespan. By P8 the ubiquitinated protein levels in the AMSH$^{-/-}$ brain had increased markedly. These data suggest that AMSH deficiency leads to the progressive accumulation of ubiquitinated proteins in the membrane fraction of the brain.

Histopathological examination of the hippocampus, the brain region most affected in AMSH$^{-/-}$ mice, showed evident neurodegeneration in the CA1 subfield in P6 mice [8]. Confirming the pres-

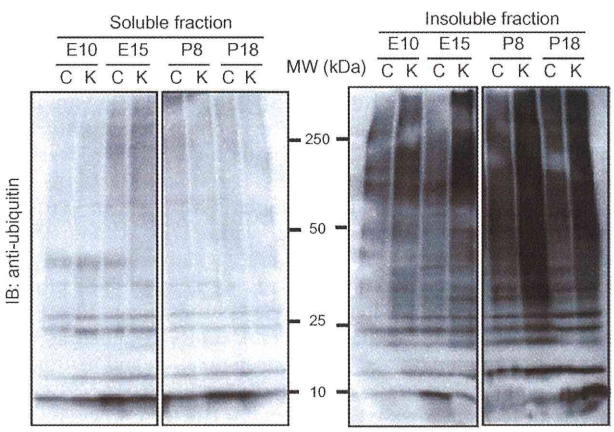

Fig. 1. Ubiquitinated proteins increase with aging in the AMSH knockout mouse brain. Western blots were performed on soluble and insoluble brain fractions of control (C) and AMSH knockout (K) mice at the ages indicated (see Section 2) using the anti-ubiquitin antibody P4D1. Gels were loaded with equal amounts of protein. IB, immunoblotting.

Please cite this article in press as: S. Suzuki et al., AMSH is required to degrade ubiquitinated proteins in the central nervous system, Biochem. Biophys. Res. Commun. (2011), doi:10.1016/j.bbrc.2011.04.065

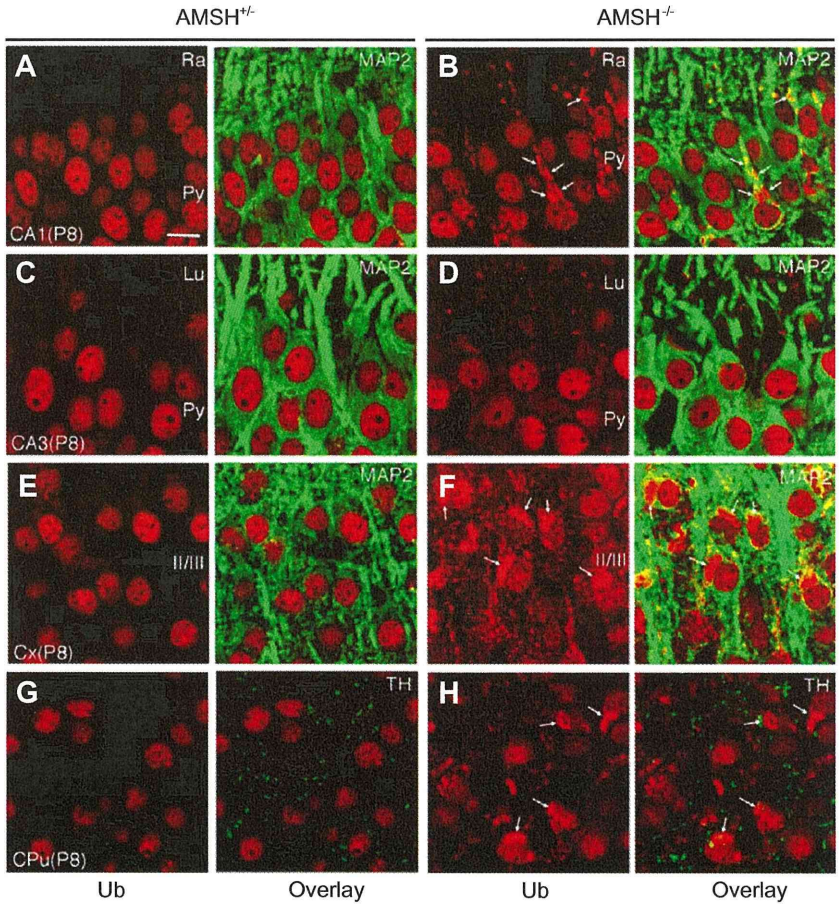

Fig. 2. Ubiquitinated proteins accumulate in the AMSH$^{-/-}$ mouse neurons. Immunofluorescence in postnatal day 8 (P8) AMSH$^{+/-}$ and AMSH$^{-/-}$ tissues stained with antibodies against ubiquitinated proteins in red (clone FK2) is shown in the hippocampal CA1 (A and B), CA3 (C and D), cerebral cortex (E and F), and caudate putamen (G and H). Arrows indicate ubiquitin-positive aggregates. Bar, 10 μm. Lu, stratum lucidum; Py, pyramidal cell layer; Ra, stratum radiatum; II/III, laminae II/III.

ence of neural damage, staining with the glial marker GFAP (glial fibrillary acidic protein) was greater in the hippocampal CA1 subfield of the AMSH$^{-/-}$ P1 brain than in the control, and was profoundly increased in P8 mice (data not shown). To determine whether ubiquitin is involved in the neuronal degeneration observed in AMSH$^{-/-}$ mice, we immunostained brain tissues with FK2, an antibody against ubiquitinated protein. In P8 AMSH$^{-/-}$ brains, FK2-stained granules were clearly apparent in the CA1 subfield, frontal cortex (Cx), and caudate putamen (CPu), but not in the CA3 subfield (Fig. 2A to H in red). The immunostainings of microtubule-associated protein 2 and ubiquitined aggregate were colocalized in CA1 and Cx (Fig. 2A–F). The staining patterns both dopaminergic (tyrosine hydroxylase-positive) fibers in CPu were similar between control and AMSH$^{-/-}$ mice (Fig. 2G and H). The ubiquitinated aggregates in CPu were partially colocalized with dopaminergic fibers, which suggested that ubiquitinated proteins did not accumulated in dopaminergic neurons but in the striatal neurons receiving dopaminergic input. These results suggested that both the ubiquitinated protein accumulation and neuron loss specifically occurred in the AMSH$^{-/-}$ CA1 subfield.

We next examined whether the AMSH deficiency impacts autophagy. Because AMSH is generally known to interact with ESCRT protein components [16], and ESCRT is closely involved with the autophagic pathway [12,17], insufficient autophagy and autophagic protein clearance might account for the aggregation of ubiquitinated proteins in the AMSH$^{-/-}$ mouse brain. We therefore looked at two marker proteins for autophagy: LC3, a specific autophagosome marker, and p62, a ubiquitin-binding protein that is implicated in autophagic protein degradation and that accumulates intracellularly with insufficient autophagy [18]. Although LC3-positive vesicles could not be detected at P20 in either the control or AMSH$^{-/-}$ brain (data not shown), p62 aggregations were clearly observed in pyramidal cell perikarya in the CA1 subfield, Cx, and CPu in the AMSH$^{-/-}$ brain (Fig. 3A and B in red[1] and data not shown). Notably, p62 and ubiquitinated proteins colocalized strongly.

We next examined the expression of the transactivation response element (TAR)-DNA-binding protein 43 (TDP-43), since a previous report suggested that defective ESCRT function leads to aggregations of cytoplasmic proteins, including TDP-43 [19]. Interestingly, TDP-43 was found in several regions of the AMSH$^{-/-}$ P8 brain, including the CA1 subfield, Cx, and CPu (Fig. 3E and F in green and data not shown), and its levels increased markedly from P8 to P20 (Fig. 3G and H). TDP-43 accumulations did not colocalize with ubiquitinated proteins (Fig. 3F), but rather with GFAP (Fig. 3D). These data indicate that TDP-43 accumulates in astrocytes but not neural cells in AMSH$^{-/-}$ mice.

AMSH is known to deubiquitinate receptors, such as the EGF receptor [5] and protease-activated receptor 2 [20], but how AMSH contributes to receptor deubiquitination *in vivo* is unknown. We

[1] For interpretation of color in Figs. 2 and 3, the reader is referred to the web version of this article.

Please cite this article in press as: S. Suzuki et al., AMSH is required to degrade ubiquitinated proteins in the central nervous system, Biochem. Biophys. Res. Commun. (2011), doi:10.1016/j.bbrc.2011.04.065

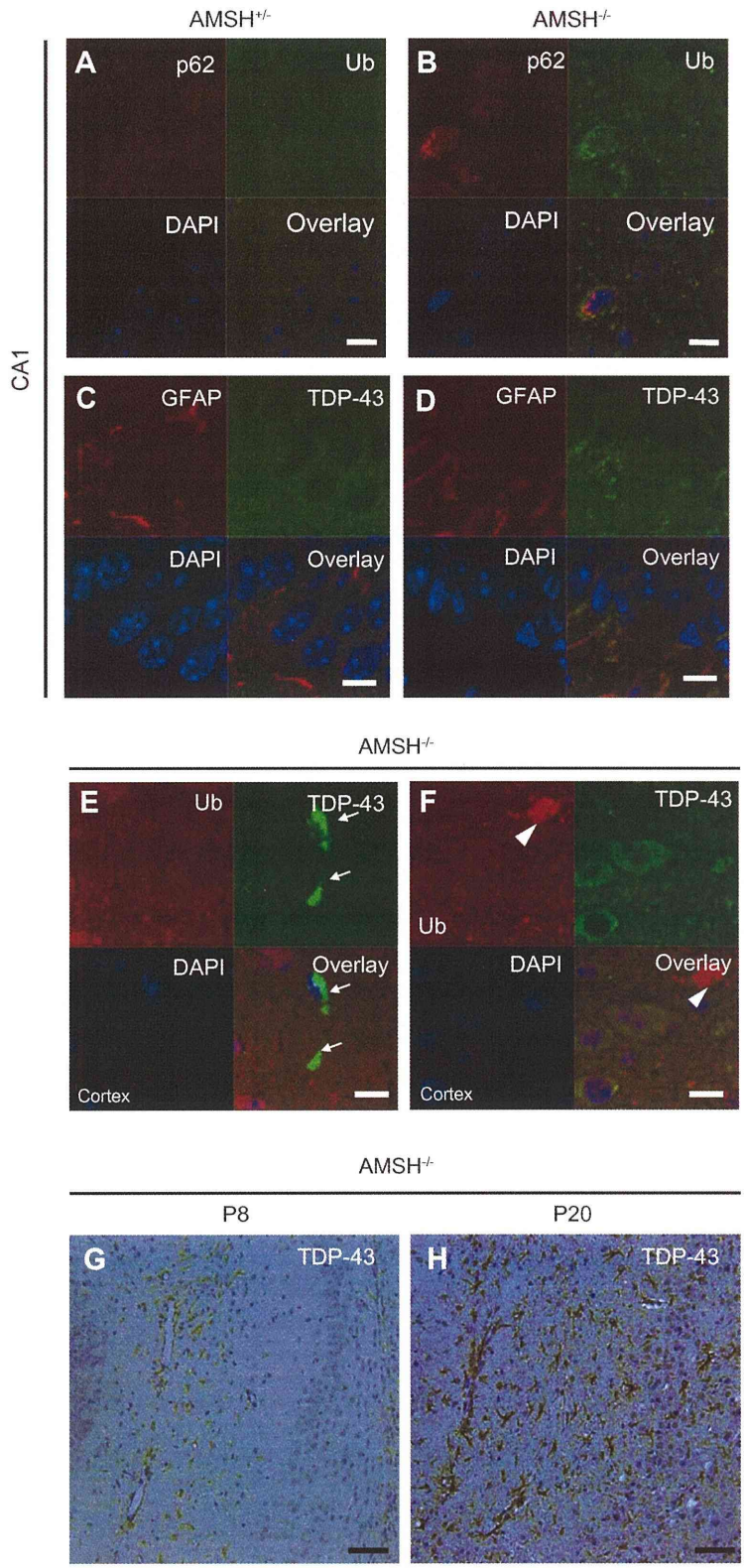

Fig. 3. Ubiquitinated proteins, p62, and TDP-43 accumulate in the AMSH$^{-/-}$ mouse brain. (A and B) Immunofluorescence in P20 AMSH$^{+/-}$ and AMSH$^{-/-}$ tissues stained with antibodies against ubiquitinated proteins (1B3) and p62 is shown in the hippocampal CA1. (C and D) TDP-43 and GFAP colocalize in the AMSH$^{-/-}$ mouse brain. Immunofluorescence staining with antibodies against GFAP and TDP-43 in AMSH$^{+/-}$ and AMSH$^{-/-}$ mice at P20 in the hippocampal CA1 subfield. Bar, 10 μm. (E and F) Immunofluorescence staining in the cerebral cortex of P20 AMSH$^{+/-}$ and AMSH$^{-/-}$ mice, using antibodies against ubiquitinated proteins (1B3) and TDP-43. Arrows indicate TDP-43-positive cells. Arrowheads indicate ubiquitin-positive cells. Bar, 10 μm. (G and H) Immunohistochemistry of hippocampal CA1 subfields from AMSH$^{-/-}$ mice at P8 (E) and P20 (F), stained with an anti-TDP-43 antibody. Bar, 50 μm.

Please cite this article in press as: S. Suzuki et al., AMSH is required to degrade ubiquitinated proteins in the central nervous system, Biochem. Biophys. Res. Commun. (2011), doi:10.1016/j.bbrc.2011.04.065

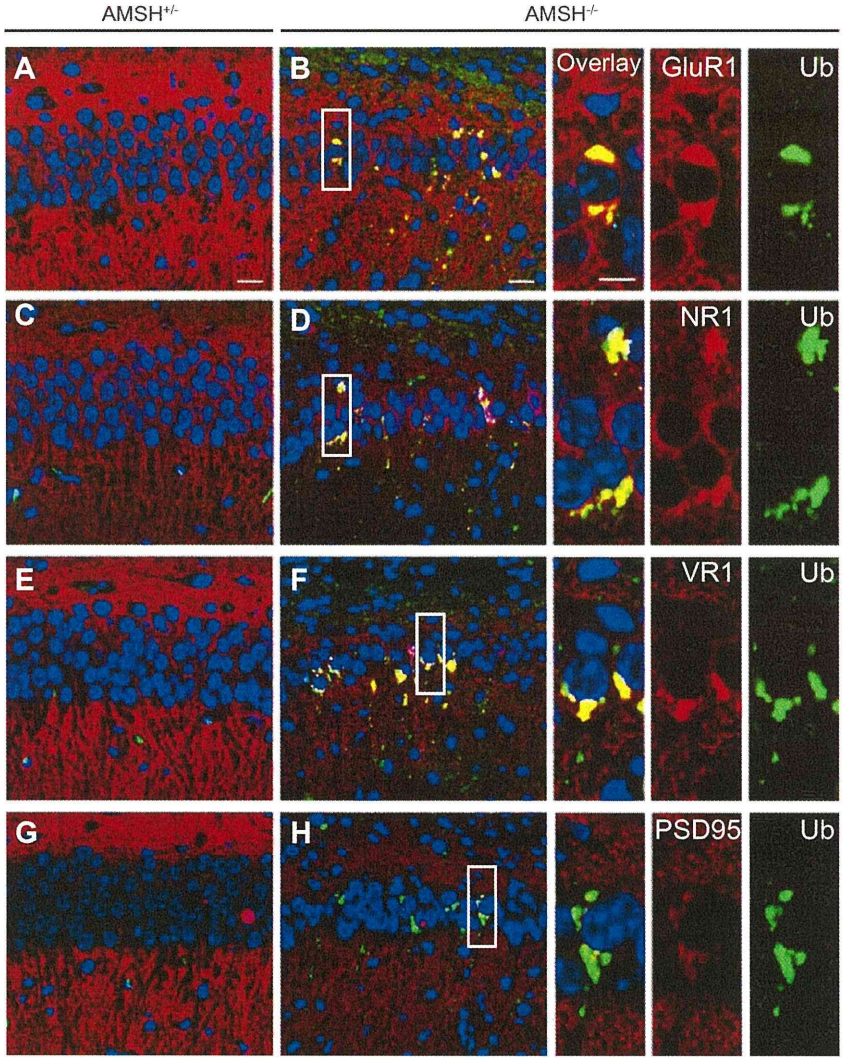

Fig. 4. Patterns of glutamate receptor subunits and ubiquitinated proteins. Immunofluorescence reactions in P8 AMSH$^{+/-}$ (A, C, E, G) and AMSH$^{-/-}$ (B, D, F, H) mice are shown. CA1 subfields were counterstained with DAPI (blue) and stained with antibodies (red) against GluR1 (A and B), NR1 (C and D), VR1 (E and F), and PSD95 (G and H). Ubiquitinated proteins were also stained in green.

suspected that glutamate receptors, which play prominent roles in several neurodegenerative diseases [21], might be regulated by AMSH. We used immunohistochemistry to examine the expression and localization of GluR1, which is a subunit of the α-amino-3-hydroxy-5-methyl-isoxazolepropionic acid receptor (AMPAR), as well as NR1 and VR1, which are subunits of the *N*-methyl-D-aspartate receptor (NMDAR), in the CA1 subfield. Aggregates in the AMSH$^{+/-}$ brain were not stained by antibodies against GluR1, NR1, or VR1 (Fig. 4A, C, E, and G); however, glutamate receptor-positive aggregates were clearly visible (Fig. 4B, D, F, and H). PSD95, which is known to bind Hrs and control glutaminergic synapse function, was weakly detected and was found colocalized with ubiquitinated proteins. Interestingly, we found the colocalization of glutamate receptor- and ubiquitin-positive aggregates (Fig. 4B, D, F, and H, insets). These results indicate that AMSH is critical for glutamate receptor regulation.

4. Discussion

The present study demonstrated that ubiquitinated proteins were accumulated in the membranous fractions of the AMSH-deficient mouse brain, indicating that membrane traffic is altered. These accumulations were found as early as E10. In a previous study, we found neuron loss in the AMSH-deficient CA1 subfield on and after P8, but not at E19 or P1 [8]. Ubiquitinated protein aggregates in neurons are known to induce neurodegeneration in conditions such as AD, FTD, and ALS [9]. Therefore, it is reasonable that we detected aggregates of ubiquitinated proteins prior to neurodegeneration in the AMSH-deficient brain. Ubiquitinated proteinaceous aggregates in the brains of AMSH-knockout mice colocalized with p62, which also accumulates in the affected neurons. The protein p62 binds ubiquitin and the autophagosome marker protein LC3, and regulates aggregate formation [22]. In addition, p62 is a selective target of autophagy, and is eventually degraded in lysosomes as a result of the autophagosome-lysosome fusion event [22]. Based on these findings, it is possible that AMSH is required for the basal or naturally occurring autophagic clearance of aggregate-prone proteins by facilitating the autophagosome-lysosome fusion.

We also observed TDP-43 aggregates in GFAP-positive glial cells in the AMSH-deficient brain, and these aggregates were not stained by anti-ubiquitin antibodies. In contrast, TDP-43 has been

Please cite this article in press as: S. Suzuki et al., AMSH is required to degrade ubiquitinated proteins in the central nervous system, Biochem. Biophys. Res. Commun. (2011), doi:10.1016/j.bbrc.2011.04.065

reported to accumulate in cytoplasmic lesions in neural cells and to colocalize with ubiquitin-positive cellular inclusions in human neurodegenerative diseases such as ALS and FTD [23]. However, a recent study showed that neuronal and glial inclusions were positively stained with ubiquitin and TDP-43 antibodies in some FTD brain specimens [24]. As TDP-43 is known to be polyubiquitinated in the presence of proteasome inhibitors [25], we expected AMSH to be critical for degrading TDP-43 in glial cells. However, we failed to detect TDP-43 ubiquitination in glial cells. Furthermore, we also examined alpha-synuclein, one of the proteins affected in PD, and phosphorylated Tau, which accumulates in AD, and found no differences between the $AMSH^{+/-}$ and $AMSH^{-/-}$ brains (data not shown). These results suggest that there may be an unknown substrate that needs to be cleared by AMSH-dependent deubiquitination and sorting, or that AMSH may be required for non-specific clearance of unwanted proteins. Further study is required to find AMSH substrates related to neurodegenerative disease.

In contrast to our present findings of neurodegeneration in the CA1 subfield in AMSH knockout mice, we previously reported finding CA3 sector neurodegeneration in STAM1-knockout as well as neuron-specific Hrs-knockout mice [12,26]. STAM1 and Hrs form an ESCRT-0 complex, which sorts ubiquitinated proteins upstream of ESCRT-III [27]. The mechanism determining the specificity of neurodegeneration in CA1 versus CA3 is an intriguing issue. Since AMSH and Hrs are distributed ubiquitously in the hippocampus, including the CA1 and CA3 subfields [8,12], their expression patterns do not account for the difference. The glutamate receptor subunit aggregates that we found in the CA1 subfield of the $AMSH^{-/-}$ brain in this study have also been found in the CA3 subfield in the Hrs-knockout brain. While we cannot completely exclude the possibility that neurodegeneration itself causes the accumulations of ubiquitinated aggregates, we suspect that instead, neurodegeneration is a result of impaired glutamate receptor regulation; we found that ubiquitinated protein accumulations were already present at E10 and E15 in the $AMSH^{-/-}$ brain, before CA1 pyramidal neuron loss occurs [8]. We also suspect that the survival of hippocampal neurons in the CA1 and CA3 subfields requires novel, distinct proteins that are subject to ubiquitination. Further study is required to determine how endosomal trafficking is regulated in the different subfields in the hippocampus.

Among the ESCRT molecules, CHMP2B mutations cause chromosome 3-linked, familial FTD (FTD-3) in humans. CHMP2B is a component of ESCRT-III, and like AMSH, is recruited to the endosomes and MVB for cargo sorting. Because AMSH binds indirectly with CHMP2B via another ESCRT-III molecule, CHMP3 [28], AMSH depletion and CHMP2B mutations seem to share similar pathological features. Indeed, neurodegeneration in FTD-3 patients is distributed not only in the frontal, parietal and temporal cortex, but also in the hippocampus. Histopathological changes found in patients with late stages of ubiquitin-positive FTD include changes in the CA1 sector of the hippocampus [29]. In addition, p62 and ubiquitinated protein accumulations are related to human neurodegenerative diseases [18]. It is not known whether AMSH selectively recognizes harmful gene products associated with neurodegenerative disorders. However, AMSH mutant mice provide an excellent animal model system for studying the molecular mechanisms of neurodegenerative diseases.

Acknowledgments

This work was supported by JSPS and MEXT KAKENHI (21590517, 19059001, and 22790630), by a Grant-in-Aid from the Ministry of Health, Labor and Welfare, by Takeda Medical Research Foundation, and by Intelligent Cosmos Research Institute.

References

[1] J.H. Hurley, S.D. Emr, The ESCRT complexes: structure and mechanism of a membrane-trafficking network, Annu. Rev. Biophys. Biomol. Struct. 35 (2006) 277–298.
[2] S.M. Nijman, M.P. Luna-Vargas, A. Velds, T.R. Brummelkamp, A.M. Dirac, T.K. Sixma, R. Bernards, A genomic and functional inventory of deubiquitinating enzymes, Cell 123 (2005) 773–786.
[3] P.C. Evans, Regulation of pro-inflammatory signalling networks by ubiquitin: identification of novel targets for anti-inflammatory drugs, Expert Rev. Mol. Med. 7 (2005) 1–19.
[4] N. Tanaka, K. Kaneko, H. Asao, H. Kasai, Y. Endo, T. Fujita, T. Takeshita, K. Sugamura, Possible involvement of a novel STAM-associated molecule "AMSH" in intracellular signal transduction mediated by cytokines, J. Biol. Chem. 274 (1999) 19129–19135.
[5] J. McCullough, M.J. Clague, S. Urbe, AMSH is an endosome-associated ubiquitin isopeptidase, J. Cell Biol. 166 (2004) 487–492.
[6] M. Kyuuma, K. Kikuchi, K. Kojima, Y. Sugawara, M. Sato, N. Mano, J. Goto, T. Takeshita, A. Yamamoto, K. Sugamura, N. Tanaka, AMSH, an ESCRT-III associated enzyme, deubiquitinates cargo on MVB/late endosomes, Cell Struct. Funct. 31 (2007) 159–172.
[7] M. Agromayor, J. Martin-Serrano, Interaction of AMSH with ESCRT-III and deubiquitination of endosomal cargo, J. Biol. Chem. 281 (2006) 23083–23091.
[8] N. Ishii, Y. Owada, M. Yamada, S. Miura, K. Murata, H. Asao, H. Kondo, K. Sugamura, Loss of neurons in the hippocampus and cerebral cortex of AMSH-deficient mice, Mol. Cell. Biol. 21 (2001) 8626–8637.
[9] C.A. Ross, M.A. Poirier, Protein aggregation and neurodegenerative disease, Nat. Med. 10 (Suppl.) (2004) S10–S17.
[10] J.A. Lee, A. Beigneux, S.T. Ahmad, S.G. Young, F.B. Gao, ESCRT-III dysfunction causes autophagosome accumulation and neurodegeneration, Curr. Biol. 17 (2007) 1561–1567.
[11] G. Skibinski, N.J. Parkinson, J.M. Brown, L. Chakrabarti, S.L. Lloyd, H. Hummerich, J.E. Nielsen, J.R. Hodges, M.G. Spillantini, T. Thusgaard, S. Brandner, A. Brun, M.N. Rossor, A. Gade, P. Johannsen, S.A. Sorensen, S. Gydesen, E.M. Fisher, J. Collinge, Mutations in the endosomal ESCRTIII-complex subunit CHMP2B in frontotemporal dementia, Nat. Genet. 37 (2005) 806–808.
[12] K. Tamai, M. Toyoshima, N. Tanaka, N. Yamamoto, Y. Owada, H. Kiyonari, K. Murata, Y. Ueno, M. Ono, T. Shimosegawa, N. Yaegashi, M. Watanabe, K. Sugamura, Loss of hrs in the central nervous system causes accumulation of ubiquitinated proteins and neurodegeneration, Am. J. Pathol. 173 (2008) 1806–1817.
[13] C. Raiborg, H. Stenmark, The ESCRT machinery in endosomal sorting of ubiquitylated membrane proteins, Nature 458 (2009) 445–452.
[14] E. Miura, M. Fukaya, T. Sato, K. Sugihara, M. Asano, K. Yoshioka, M. Watanabe, Expression and distribution of JNK/SAPK-associated scaffold protein JSAP1 in developing and adult mouse brain, J. Neurochem. 97 (2006) 1431–1446.
[15] S. Nakagawa, M. Watanabe, T. Isobe, H. Kondo, Y. Inoue, Cytological compartmentalization in the staggerer cerebellum, as revealed by calbindin immunohistochemistry for Purkinje cells, J. Comp. Neurol. 395 (1998) 112–120.
[16] M.J. Clague, S. Urbe, Endocytosis: the DUB version, Trends Cell Biol. 16 (2006) 551–559.
[17] M. Filimonenko, S. Stuffers, C. Raiborg, A. Yamamoto, L. Malerod, E.M. Fisher, A. Isaacs, A. Brech, H. Stenmark, A. Simonsen, Functional multivesicular bodies are required for autophagic clearance of protein aggregates associated with neurodegenerative disease, J. Cell Biol. 179 (2007) 485–500.
[18] M. Komatsu, S. Waguri, M. Koike, Y.S. Sou, T. Ueno, T. Hara, N. Mizushima, J. Iwata, J. Ezaki, S. Murata, J. Hamazaki, Y. Nishito, S. Iemura, T. Natsume, T. Yanagawa, J. Uwayama, E. Warabi, H. Yoshida, T. Ishii, A. Kobayashi, M. Yamamoto, Z. Yue, Y. Uchiyama, E. Kominami, K. Tanaka, Homeostatic levels of p62 control cytoplasmic inclusion body formation in autophagy-deficient mice, Cell 131 (2007) 1149–1163.
[19] T.E. Rusten, A. Simonsen, ESCRT functions in autophagy and associated disease, Cell Cycle 7 (2008) 1166–1172.
[20] B. Hasdemir, J.E. Murphy, G.S. Cottrell, N.W. Bunnett, Endosomal deubiquitinating enzymes control ubiquitination and down-regulation of protease-activated receptor 2, J. Biol. Chem. 284 (2009) 28453–28466.
[21] T.M. Tzschentke, Glutamatergic mechanisms in different disease states: overview and therapeutical implications – an introduction, Amino Acids 23 (2002) 147–152.
[22] S. Pankiv, T.H. Clausen, T. Lamark, A. Brech, J.A. Bruun, H. Outzen, A. Overvatn, G. Bjorkoy, T. Johansen, P62/SQSTM1 binds directly to Atg8/LC3 to facilitate degradation of ubiquitinated protein aggregates by autophagy, J. Biol. Chem. 282 (2007) 24131–24145.
[23] F. Geser, M. Martinez-Lage, L.K. Kwong, V.M. Lee, J.Q. Trojanowski, Amyotrophic lateral sclerosis, frontotemporal dementia and beyond: the TDP-43 diseases, J. Neurol. 256 (2009) 1205–1214.
[24] N.J. Cairns, M. Neumann, E.H. Bigio, I.E. Holm, D. Troost, K.J. Hatanpaa, C. Foong, C.L. White 3rd, J.A. Schneider, H.A. Kretzschmar, D. Carter, L. Taylor-Reinwald, K. Paulsmeyer, J. Strider, M. Gitcho, A.M. Goate, J.C. Morris, M. Mishra, L.K. Kwong, A. Stieber, Y. Xu, M.S. Forman, J.Q. Trojanowski, V.M. Lee, I.R. Mackenzie, TDP-43 in familial and sporadic frontotemporal lobar degeneration with ubiquitin inclusions, Am. J. Pathol. 171 (2007) 227–240.

Please cite this article in press as: S. Suzuki et al., AMSH is required to degrade ubiquitinated proteins in the central nervous system, Biochem. Biophys. Res. Commun. (2011), doi:10.1016/j.bbrc.2011.04.065

[25] M.J. Winton, L.M. Igaz, M.M. Wong, L.K. Kwong, J.Q. Trojanowski, V.M. Lee, Disturbance of nuclear and cytoplasmic TAR DNA-binding protein (TDP-43) induces disease-like redistribution, sequestration, and aggregate formation, J. Biol. Chem. 283 (2008) 13302–13309.
[26] M. Yamada, T. Takeshita, S. Miura, K. Murata, Y. Kimura, N. Ishii, M. Nose, H. Sakagami, H. Kondo, F. Tashiro, J.I. Miyazaki, H. Sasaki, K. Sugamura, Loss of hippocampal CA3 pyramidal neurons in mice lacking STAM1, Mol. Cell. Biol. 21 (2001) 3807–3819.
[27] Y. Tanaka, N. Tanaka, Y. Saeki, K. Tanaka, M. Murakami, T. Hirano, N. Ishii, K. Sugamura, C-Cbl-dependent monoubiquitination and lysosomal degradation of gp130, Mol. Cell. Biol. 28 (2008) 4805–4818.
[28] B. McDonald, J. Martin-Serrano, No strings attached: the ESCRT machinery in viral budding and cytokinesis, J. Cell Sci. 122 (2009) 2167–2177.
[29] C. Kersaitis, G.M. Halliday, J.J. Kril, Regional and cellular pathology in frontotemporal dementia: relationship to stage of disease in cases with and without Pick bodies, Acta Neuropathol. 108 (2004) 515–523.

Please cite this article in press as: S. Suzuki et al., AMSH is required to degrade ubiquitinated proteins in the central nervous system, Biochem. Biophys. Res. Commun. (2011), doi:10.1016/j.bbrc.2011.04.065

Virology 422 (2012) 377–385

Contents lists available at SciVerse ScienceDirect

Virology

journal homepage: www.elsevier.com/locate/yviro

Regulation of hepatitis C virus secretion by the Hrs-dependent exosomal pathway

Keiichi Tamai [a,b], Masaaki Shiina [b], Nobuyuki Tanaka [a,d,*], Takashi Nakano [e], Akitsugu Yamamoto [f], Yasuteru Kondo [b], Eiji Kakazu [b], Jun Inoue [b], Koji Fukushima [b], Kouichi Sano [e], Yoshiyuki Ueno [b], Tooru Shimosegawa [b], Kazuo Sugamura [a,c]

[a] Division of Cancer Biology and Therapeutics, Miyagi Cancer Center Research Institute, Natori 981-1293, Japan
[b] Department of Gastroenterology, Tohoku University Graduate School of Medicine, Sendai, 980-8575, Japan
[c] Department of Microbiology and Immunology, Tohoku University Graduate School of Medicine, Sendai, 980-8575, Japan
[d] Department of Cancer Science, Tohoku University Graduate School of Medicine, Sendai, 980-8575, Japan
[e] Department of Microbiology and Infection Control, Faculty of Medicine, Osaka Medical College, Takatsuki, Osaka 569-8686, Japan
[f] Department of Animal Bio-Science, Faculty of Bio-Science, Nagahama Institute of Bio-Science and Technology, Nagahama, 526-0829, Japan

ARTICLE INFO

Article history:
Received 14 July 2011
Returned to author for revision
6 September 2011
Accepted 10 November 2011
Available online 3 December 2011

Keywords:
Hrs
ESCRT
HCV

ABSTRACT

The molecular mechanisms of assembly and budding of hepatitis C virus (HCV) remain poorly understood. The budding of several enveloped viruses requires an endosomal sorting complex required for transport (ESCRT), which is part of the cellular machinery used to form multivesicular bodies (MVBs). Here, we demonstrated that Hrs, an ESCRT-0 component, is critical for the budding of HCV through the exosomal secretion pathway. Hrs depletion caused reduced exosome production, which paralleled with the decrease of HCV replication in the host cell, and that in the culture supernatant. Sucrose-density gradient separation of the culture supernatant of HCV-infected cells revealed the co-existence of HCV core proteins and the exosome marker. Furthermore, both the core protein and an envelope protein of HCV were detected in the intraluminal vesicles of MVBs. These results suggested that HCV secretion from host cells requires Hrs-dependent exosomal pathway in which the viral assembly is also involved.

© 2011 Elsevier Inc. All rights reserved.

Introduction

Hepatitis C virus (HCV) is a major cause of chronic liver disease, with about 170 million people infected worldwide. It is important to identify the molecular basis of HCV infection, propagation, and pathogenesis in humans. HCV is a positive-strand RNA virus belonging to the *Flaviviridae* family and the sole member of the genus *Hepacivirus*. The HCV RNA genome serves as a template for viral replication and as a messenger RNA for viral production. It is translated into a single immature polyprotein of approximately ~3000 amino acids that is further cleaved into at least 10 mature proteins by proteases (Asselah et al., 2009).

The HCV life cycle starts with virion attachment, especially through its envelope glycoproteins E1 and E2, to specific receptors on the host cells, which include CD81, claudin-1, and the class B member I scavenger receptor (Evans et al., 2007; Murray et al., 2008). These receptors and co-receptors are also required for HCV entry, which involves an additional clathrin-mediated post-internalization step and delivery into early endosomes (Burlone and Budkowska, 2009). Recently, the complete replication of HCV in a cell culture system was achieved (Wakita et al., 2005). Nevertheless, little is known about how the assembled HCV virion is released from the cytoplasm.

Extensive research on human immunodeficiency virus (HIV) has shown that the ESCRT (endosomal sorting complex required for transport) machinery plays a crucial role in virion assembly and budding from cellular membranes: The late-domain (L-domain) motif of HIV-Gag binds TSG101 (an ESCRT-I component) and Alix (a protein that bridges ESCRT-I and ESCRT-III). Virion assembly, budding, and release are subsequently achieved with help from the sequential downstream ESCRT machinery (Chen and Lamb, 2008). Other enveloped viruses, such as hepatitis B virus and human T-cell leukemia virus type I, also hijack the cellular membrane trafficking and sorting networks to accumulate and assemble their viral components, after which the nascent virions pinch themselves off for release (Chen and Lamb, 2008).

Similar to an enveloped virus particle that buds from the host-cell surface, small vesicles, called exosomes, are physiologically secreted from a variety of cells (Denzer et al., 2000; van Niel et al., 2006). Exosomes are nanovesicles (60–90 nm in diameter) surrounded by a

Abbreviations: ER, endoplasmic reticulum; ESCRT, endosomal sorting complex required for transport; HCV, hepatitis C virus; HHV-6, human herpes virus-6; HIV, human immunodeficiency virus; ILV, intraluminal vesicle L-domain, late-domain; MVB, multivesicular body; shRNA, short hairpin RNA.

* Corresponding author at: Division of Cancer Biology and Therapeutics, Miyagi Cancer Center Research Institute, 47-1 Nodayama, Medeshima-Shiode, Natori, Miyagi, 981-1293, Japan. Fax: +81 22 381 1168.
E-mail address: tanaka@med.tohoku.ac.jp (N. Tanaka).

0042-6822/$ – see front matter © 2011 Elsevier Inc. All rights reserved.
doi:10.1016/j.virol.2011.11.009

lipid bilayer. They are generated as intraluminal vesicles (ILVs) within a sorting endosome called a multivesicular body (MVB), by the inward budding of the MVB's limiting membrane. Exosome release into the extracellular milieu is achieved by direct fusion of the MVB with the plasma membrane (Pan et al., 1985).

The sorting of ubiquitinated proteins on MVBs is mediated by the ESCRT pathway. The first complex that binds the cargo on endosomes is ESCRT-0 which includes Hrs (Asao et al., 1997; Komada and Kitamura, 1995) and STAMs, and with the help of ESCRTs-I, -II, and -III, the cargo accumulates on the endosomal membrane. At the end

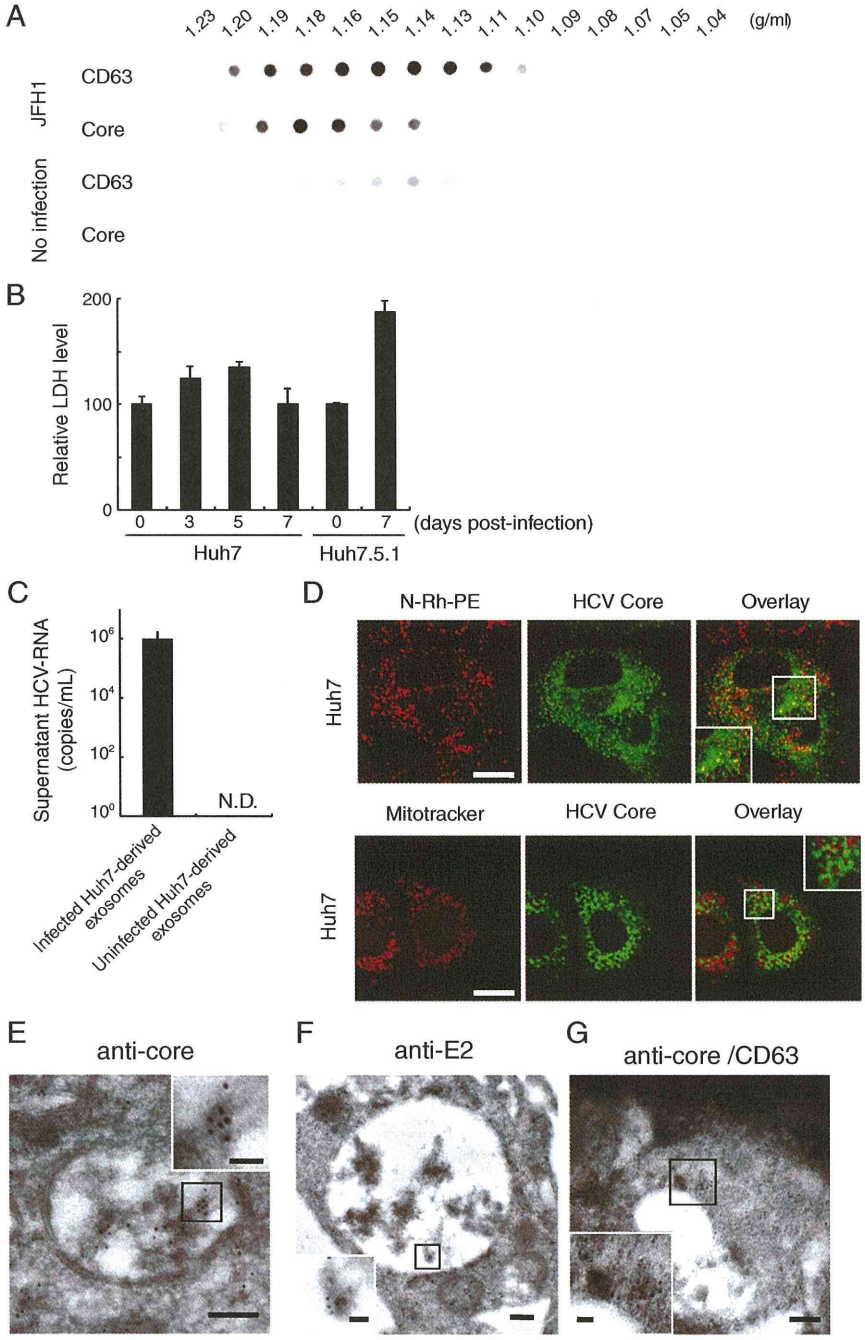

Fig. 1. Localization of HCV protein to exosome-rich fractions. (A) Dot blot analysis of the supernatants of JFH-1-infected Huh7 cells fractionated on a sucrose gradient and examined for an exosome protein (CD63) and HCV core protein. Huh7 cells were uninfected or infected with JFH-1 (MOI = 0.01), and the medium was changed after 3 days. The cells were then incubated for 2 days, and the culture supernatants were harvested and purified by ultracentrifugations. (B) Huh7 cells were infected at a multiplicity of infection of 0.01 with HCV and Lactate dehydrogenase was quantitated in culture supernatants. (C) HCV-RNA in the culture supernatant at day 5 post-infection after infection with purified exosomes from infected and uninfected Huh7 cells, measured using real-time PCR. Purified exosomes were obtained from 10 ml of supernatant of Huh7 cells at day 5 post-infection. N.D., not detectable. (D) Upper panel: Confocal microscopic image of Huh7 cells infected with JFH-1. The exosome and MVB marker, N-Rh-PE (red) and the HCV core protein (green) were partially colocalized. Lower panel: anti-core protein (green) and Mitotracker (red) were used. Bar, 20 μm. (E and F) Immunoelectron microscopy of an MVB in wild-type Huh7 cells. Sections of Huh7 cells were incubated with antibodies against HCV core protein (5-nm-colloidal-immunogold-labeled anti-mouse goat IgG in E) and HCV envelope protein E2 (5-nm in F). Insets show a higher magnification. Bars: 200 nm, bars in insets: 50 nm. (G) Double-staining of immunoelectron microscopy using antibodies against HCV core protein (10 nm) and anti-CD63 (5 nm). Insets show a higher magnification. Bars: 200 nm, bars in insets: 50 nm.

of sorting, an AAA-type ATPase, VPS4, disrupts the ESCRT complexes, and the membrane with its accumulated cargo is invaginated into the maturing endosome to produce an MVB. A deficiency of Hrs results in abnormally enlarged endosomes and a marked reduction in cargo sorting to MVBs. The enlarged endosomes accumulate ligand-activated membrane-bound growth factor receptors (Tanaka et al., 2008). In this context, we recently demonstrated that Hrs is also required in dendritic cells for exosome secretion and antigen presentation via exosomes (Tamai et al., 2010).

Relationships are also reported between membrane trafficking and the HCV life cycle. ESCRT-III contributes to HCV release in Huh7 cells (Ariumi et al., 2011; Corless et al., 2010), as does transfection of these cells with RNAi against Atg7, an essential autophagy gene (Tanida et al., 2009). Another study suggested that human plasma contains exosomes and that in HCV patients, viral RNA is associated with these circulating vesicle (Masciopinto et al., 2004). Since Hrs, an ESCRT-0 component, is involved in the autophagic pathway (Tamai et al., 2007) and required for exosome secretion, we hypothesized that Hrs plays a role in the HCV life cycle. Here we demonstrated that the Hrs-dependent exosomal pathway plays an important role in HCV release.

Results

HCV core protein localizes to exosome-rich fractions

A relationship between virus production and the exosome pathway has been suggested for HIV and human herpes virus 6 (HHV6) (Lenassi et al.; Mori et al., 2008). We suspected that HCV also utilizes the exosome pathway for its release from host cells. To examine this possibility, we subjected the culture supernatants of HCV JFH-1-infected Huh7 cells to sucrose density gradient centrifugation and analyzed the fractions for exosomes and HCV. Interestingly, the identical fractions were positive both for the exosome marker CD63 and for the HCV core protein (Fig. 1A). Notably, more CD63-positive exosomes were found in the HCV-infected Huh7 cells than in uninfected cells. To exclude a possibility that the cytopathic effect (CPE) induced by the infection of JFH-1 affects the amount of CD63 in the supernatant, we monitored the CPE by the lactate dehydrogenase (LDH) assay. In Huh7 cells, we observed slight increase of LDH at post-infection day 5 (Fig. 1B). As a positive control, we also investigated the CPE in Huh7.5.1, which is more susceptible to JFH-1 infection. LDH level was approximately two-times higher in this Huh7.5.1 cells than the non-infected, which is compatible with a previous report (Shiina and Rehermann, 2008). Purified exosomes from the culture supernatant of JFH-1-infected Huh7 cells possessed HCV-infectivity to Huh7 cells (Fig. 1C). These results indicated that the exosome secretion was mainly activated during HCV infection.

We next addressed whether HCV localizes to the intraluminal vesicles within the MVBs of JFH-1-infected Huh7 cells. Using confocal microscopy, we found that N-Rh-PE-positive dots (an exosome and MVB marker) were likely to colocalize with HCV-core-positive dots (Fig. 1D, upper panels). As a negative control, immunofluorescence staining was performed with anti-HCV-core and mitochondrial marker (Mitotracker (Molecular Probes)), which reportedly do not colocalize with each other (Lai et al., 2010). We did observe that HCV-core protein was not colocalized to mitochondria (Fig. 1D, lower panels). By immunoelectron microscopy, we detected positive immunogold staining for the HCV core antigen on the intraluminal vesicles (Fig. 1E). Similarly, positive immunogold staining for the HCV envelope protein E2 was observed on intraluminal vesicles within MVBs (Fig. 1F). To make the relationships between HCV particles and exosomes clearer, we performed the double-staining of immunoelectron microscopy using anti-CD63 and anti-core protein. We observed the colocalization of CD63 and HCV-core in the intraluminal vesicles in the MVB (Fig. 1G). These data together suggested that HCV virions and exosomes are present in the same or very similar compartments.

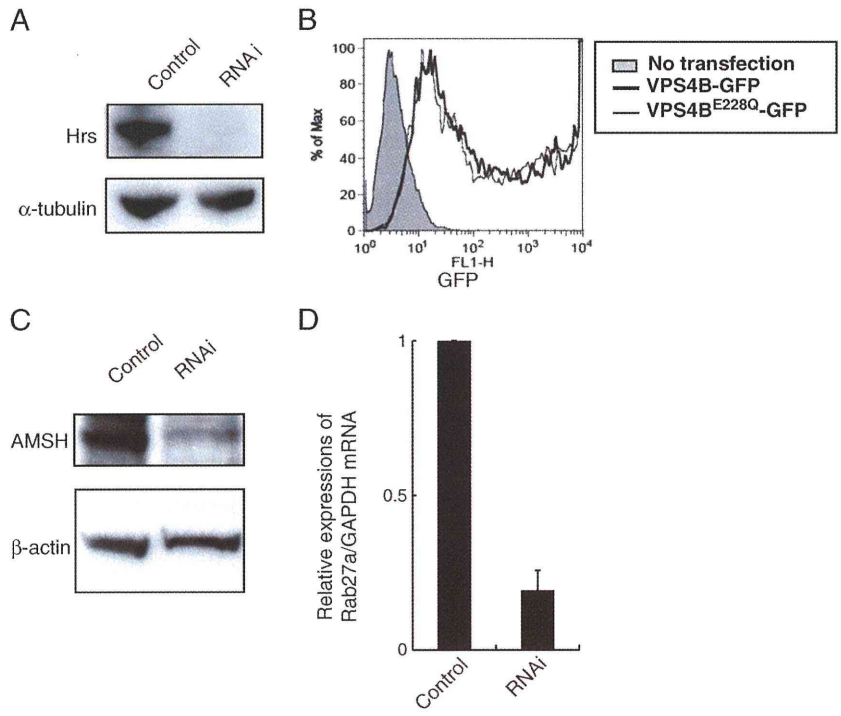

Fig. 2. Establishment of Huh7 lines with knocked-down Hrs, AMSH or Rab27a, and overexpressed VPS4B. (A) Western blot analysis of total-cell lysates from control and Hrs (A) and AMSH (C) knock-down Huh7 cells. (B) Flow-cytometry analysis of Huh7 cells overexpressing GFP-fused VPS4B (wild-type and dominant-negative (E228Q) forms). (D) Quantitative real-time PCR analysis of Rab27a in Huh7 cells. Rab27a mRNA expression was normalized to GAPDH.